Inter-basin versus intra-basin sea surface temperature forcing of the Western North Pacific subtropical high's westward extensions

Jhordanne Jones[1], Daniel Chavas[1], and Zachary Freitag Johnson[2]

[1]Purdue University
[2]Central Michigan University

November 22, 2023

Abstract

Zonal extensions of the Western Pacific subtropical high (WPSH) strongly modulate extreme rainfall activity and tropical cyclone (TC) landfall over the Western North Pacific (WNP) region. On seasonal timescales, these zonal extensions are forced primarily by inter-basin zonal sea surface temperature (SST) gradients. However, despite the presence of large-scale zonal SST gradients, the WPSH's response to SSTs varies from year to year. In this study, we force the atmosphere-only NCAR Community Earth System Model version 2 simulations with two real-world SST patterns, both featuring the large-scale zonal SST gradient characteristic of decaying El Niño/developing La Niña summers. For each of these patterns, we perform four experimental sets that test the relative contributions of the tropical Indian Ocean, Pacific, and Atlantic basin SSTs to simulated westward extensions over the WNP during June-August. Our results indicate that the subtle differences between the two SST anomaly patterns belie two different mechanisms forcing the WPSH's westward extensions. In one SST pattern, the extratropical North Pacific SST forcing suppresses the tropical Pacific zonal SST gradient forcing, resulting in tropical Atlantic and Indian Ocean SST warming being the main drivers of the Walker Circulation. With an adjacent SST pattern, subsidence over the WNP is driven predominantly by intra-basin Pacific SST forcing. The results of this study have implications for understanding and predicting the impact of the WPSH's zonal variability on tropical cyclones and extreme rainfall over the WNP.

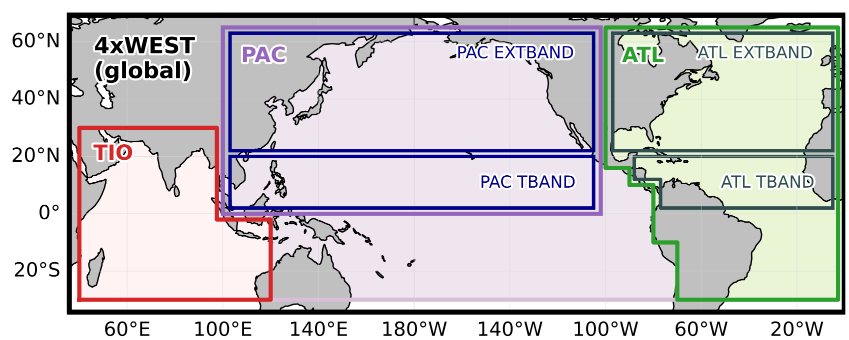

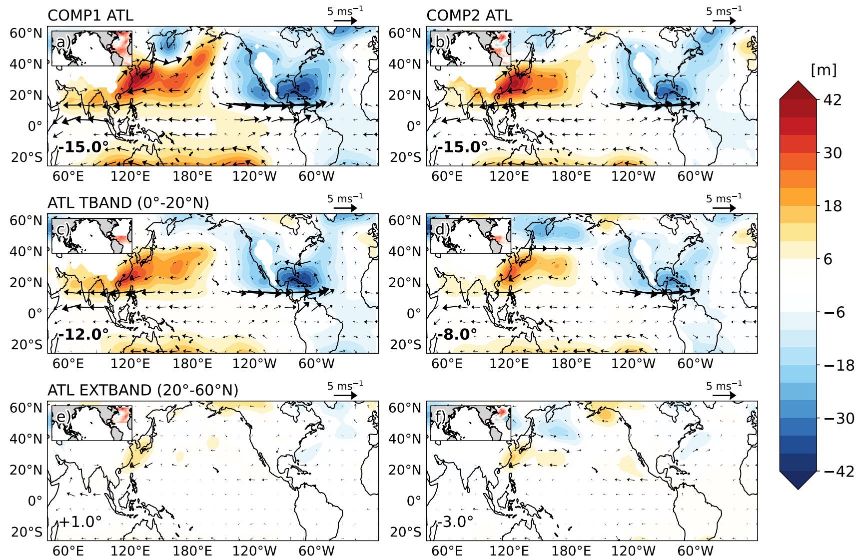
COMP1 ATL
COMP2 ATL
ATL TBAND (0°-20°N)
ATL EXTBAND (20°-60°N)
5 ms⁻¹
-15.0°
-15.0°
-12.0°
-8.0°
+1.0°
-3.0°
[m]
60°N
40°N
20°N
0°
20°S
60°E
120°E
180°E
120°W
60°W

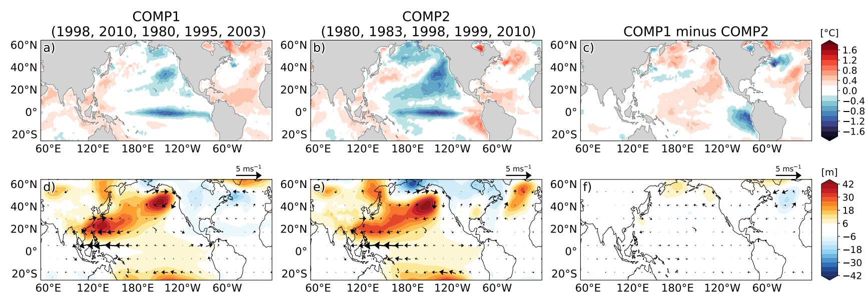
COMP1
(1998, 2010, 1980, 1995, 2003)
COMP2
(1980, 1983, 1998, 1999, 2010)
COMP1 minus COMP2
[°C]
[m]
5 ms⁻¹

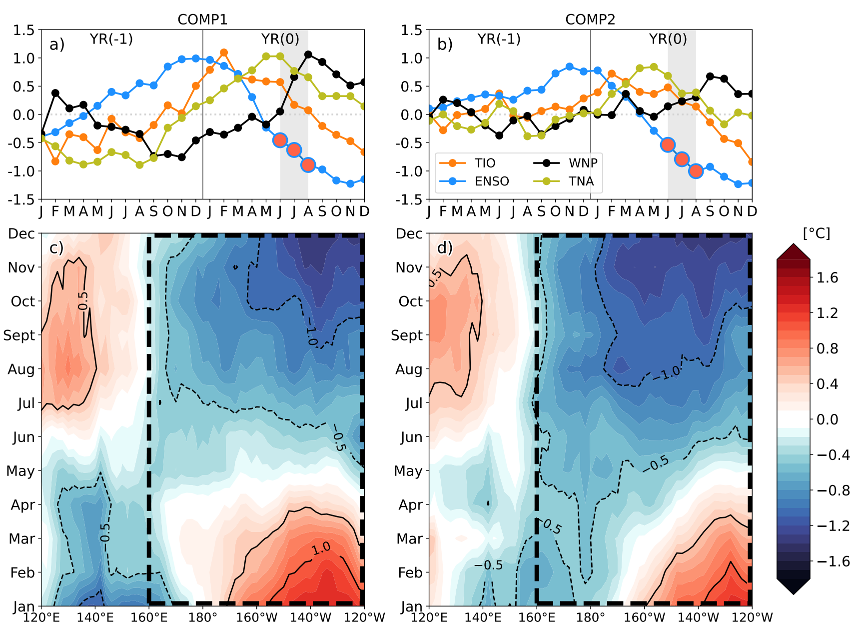
COMP1
COMP2
YR(-1)
YR(0)
TIO
ENSO
WNP
TNA
J F M A M J J A S O N D J F M A M J J A S O N D
Dec
Nov
Oct
Sept
Aug
Jul
Jun
May
Apr
Mar
Feb
Jan
120°E
140°E
160°E
180°
160°W
140°W
120°W
[°C]

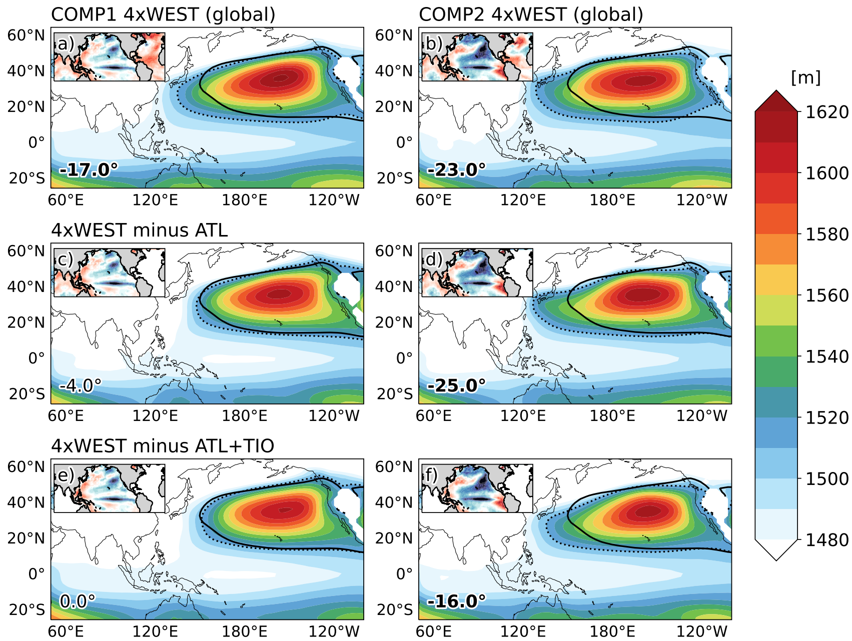
COMP1 4xWEST (global)
COMP2 4xWEST (global)
4xWEST minus ATL
4xWEST minus ATL+TIO
a)
b)
c)
d)
e)
f)
-17.0°
-23.0°
-4.0°
-25.0°
0.0°
-16.0°
[m]
1620
1600
1580
1560
1540
1520
1500
1480
60°N
40°N
20°N
0°
20°S
60°E
120°E
180°E
120°W

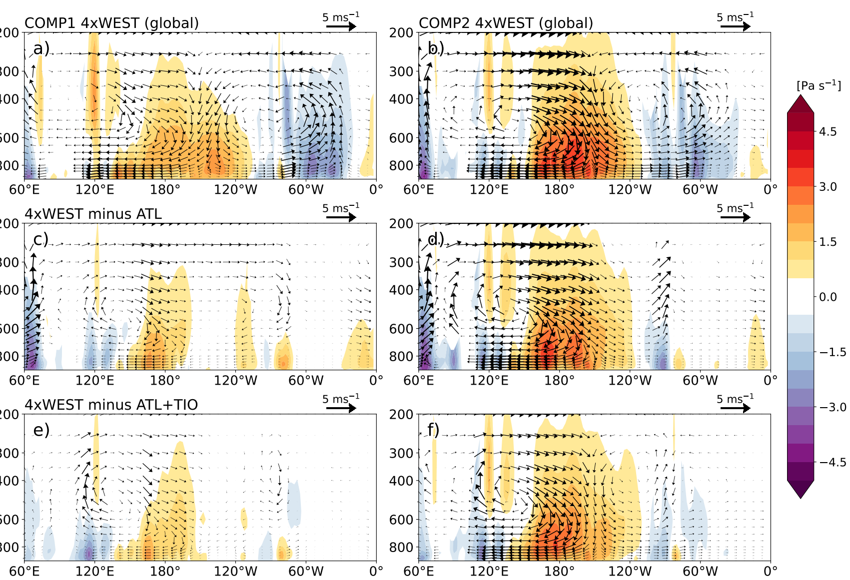
COMP1 4xWEST (global)
COMP2 4xWEST (global)
4xWEST minus ATL
4xWEST minus ATL+TIO
5 ms^{-1}
a)
b)
c)
d)
e)
f)
[Pa s^{-1}]
4.5
3.0
1.5
0.0
−1.5
−3.0
−4.5
200
300
400
600
800
60°E
120°E
180°
120°W
60°W
0°

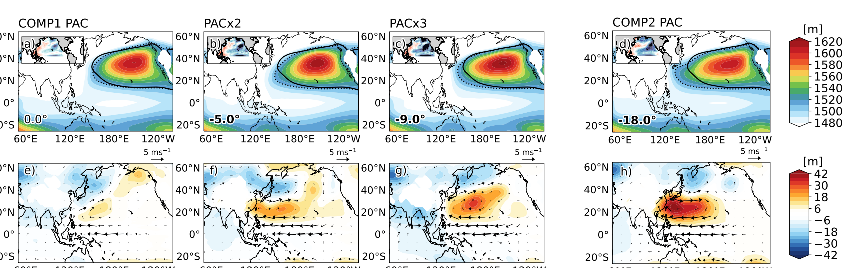
COMP1 PAC
PACx2
PACx3
COMP2 PAC
a)
b)
c)
d)
e)
f)
g)
h)
0.0°
-5.0°
-9.0°
-18.0°
5 ms^{-1}
[m]
1620
1600
1580
1560
1540
1520
1500
1480
[m]
42
30
18
6
−6
−18
−30
−42
60°N
40°N
20°N
0°
20°S
60°E
120°E
180°E
120°W

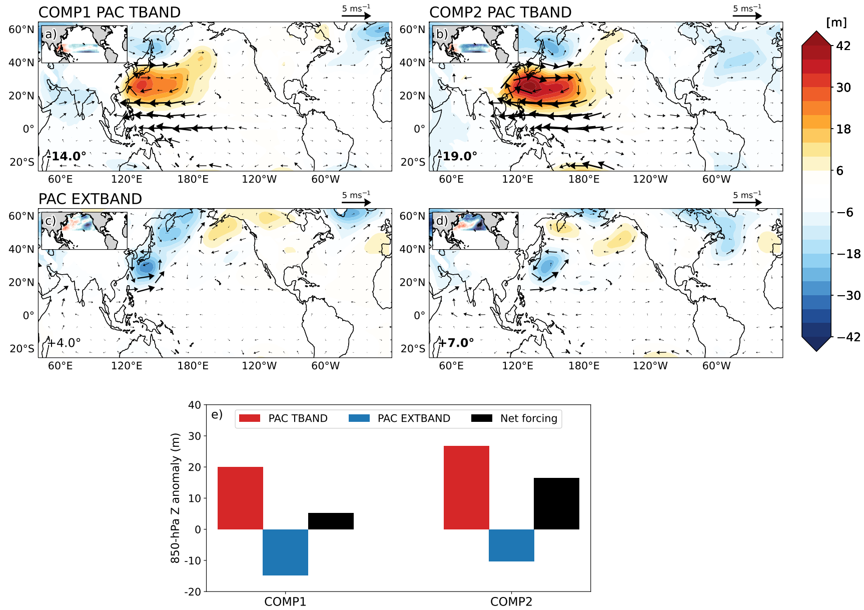
COMP1 PAC TBAND
COMP2 PAC TBAND
PAC EXTBAND
5 ms^{-1}
a)
b)
c)
d)
e)
14.0°
19.0°
+4.0°
+7.0°
60°N
40°N
20°N
0°
20°S
60°E
120°E
180°E
120°W
60°W
[m]
42
30
18
6
−6
−18
−30
−42
PAC TBAND
PAC EXTBAND
Net forcing
850-hPa Z anomaly (m)
COMP1
COMP2

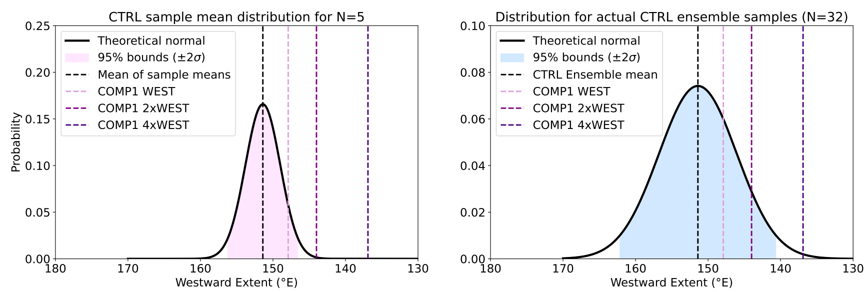
CTRL sample mean distribution for N=5
Theoretical normal
95% bounds (±2σ)
Mean of sample means
COMP1 WEST
COMP1 2xWEST
COMP1 4xWEST
Probability
Westward Extent (°E)
Distribution for actual CTRL ensemble samples (N=32)
CTRL Ensemble mean

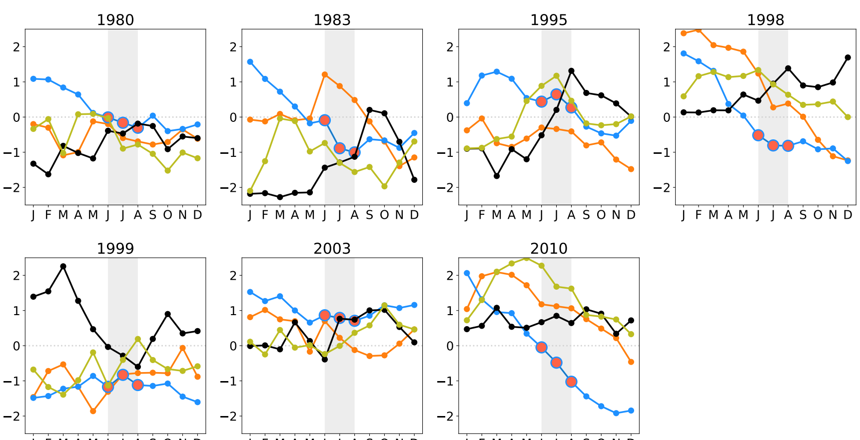
1980
1983
1995
1998
1999
2003
2010
J F M A M J J A S O N D

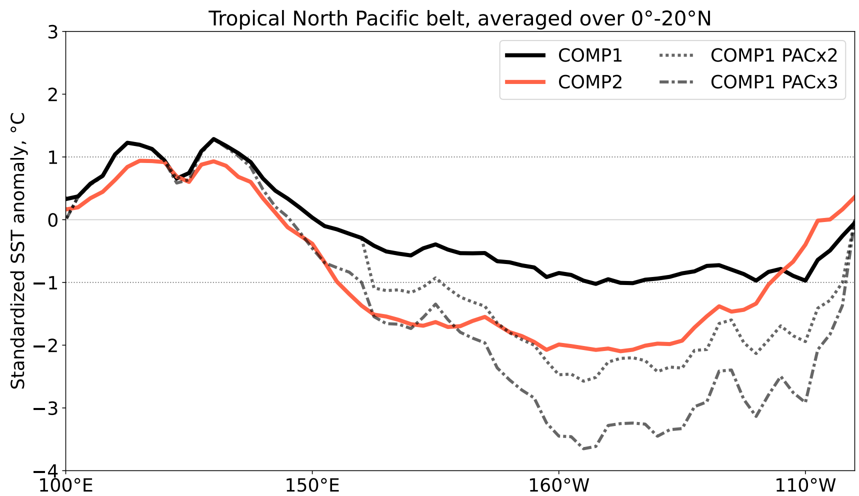
Tropical North Pacific belt, averaged over 0°-20°N
Standardized SST anomaly, °C
COMP1
COMP2
COMP1 PACx2
COMP1 PACx3
100°E
150°E
160°W
110°W

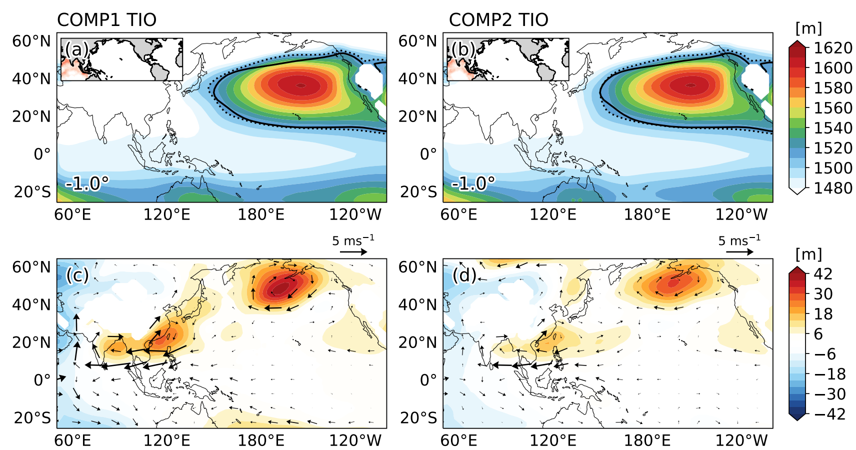
COMP1 TIO
COMP2 TIO
(a)
(b)
(c)
(d)
-1.0°
[m]
1620
1600
1580
1560
1540
1520
1500
1480
5 ms⁻¹
42
30
18
6
−6
−18
−30
−42
60°N
40°N
20°N
0°
20°S
60°E
120°E
180°E
120°W

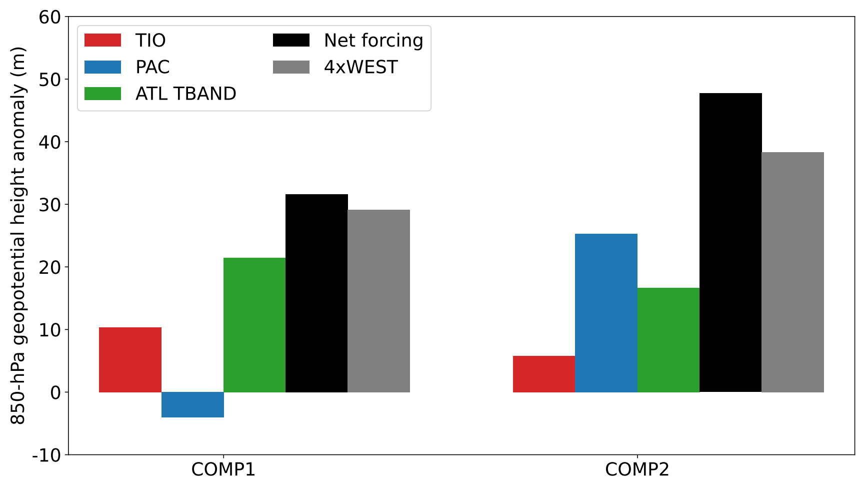
850-hPa geopotential height anomaly (m)
TIO
PAC
ATL TBAND
Net forcing
4xWEST
COMP1
COMP2

Inter-basin versus intra-basin sea surface temperature forcing of the Western North Pacific subtropical high's westward extensions

Jhordanne J. Jones[1,2*], Daniel R. Chavas[2], Zachary F. Johnson[3]

[1]University Corporation for Atmospheric Research, Boulder, CO, USA
[2]Department of Earth, Atmospheric, and Planetary Sciences, Purdue University, West Lafayette, IN, USA
[3]Department of Earth and Atmospheric Science, Central Michigan University, Mount Pleasant, MI, USA

Key Points:

- Two similar SST patterns belie two different mechanisms forcing the subtropical high"s westward extensions.
- Tropical Pacific SST gradient forcing of westward extensions can be suppressed by its extratropical SST forcing.
- Remote Atlantic SST forcing drives westward extensions when the local net Pacific forcing is weak.

*Department of Earth, Atmospheric, and Planetary Science, Purdue University

Corresponding author: Dr. Jhordanne Jones, `jjpjones@purdue.edu`

Abstract

Zonal extensions of the Western Pacific subtropical high (WPSH) strongly modulate extreme rainfall activity and tropical cyclone (TC) landfall over the Western North Pacific (WNP) region. On seasonal timescales, these zonal extensions are forced primarily by inter-basin zonal sea surface temperature (SST) gradients. However, despite the presence of large-scale zonal SST gradients, the WPSH's response to SSTs varies from year to year. In this study, we force the atmosphere-only NCAR Community Earth System Model version 2 simulations with two real-world SST patterns, both featuring the large-scale zonal SST gradient characteristic of decaying El Niño/developing La Niña summers. For each of these patterns, we perform four experimental sets that test the relative contributions of the tropical Indian Ocean, Pacific, and Atlantic basin SSTs to simulated westward extensions over the WNP during June-August. Our results indicate that the subtle differences between the two SST anomaly patterns belie two different mechanisms forcing the WPSH's westward extensions. In one SST pattern, the extratropical North Pacific SST forcing suppresses the tropical Pacific zonal SST gradient forcing, resulting in tropical Atlantic and Indian Ocean SST warming being the main drivers of the Walker Circulation. With an adjacent SST pattern, subsidence over the WNP is driven predominantly by intra-basin Pacific SST forcing. The results of this study have implications for understanding and predicting the impact of the WPSH's zonal variability on tropical cyclones and extreme rainfall over the WNP.

Plain Language Summary

Westward extensions of the Western North Pacific subtropical high (WPSH) drive rainfall extremes over the Western North Pacific basin, and is important for the prediction of summer rainfall, including monsoonal rainfall and tropical cyclone activity. Studies have previously highlighted the importance of the large-scale zonal sea surface temperature (SST) gradient - warm tropical Indian Ocean in conjunction with cold equatorial eastern Pacific Ocean - in developing and maintaining the summer WPSH and westward extensions. But, here, we show that even with very similar SST patterns, the large-scale zonal SST pattern may belie forcing from inter-basin SSTs versus intra-basin SSTs. We find that the degree of spread of negative SST anomalies across the central and eastern Pacific region may determine whether inter-basin versus intra-basin Pacific SSTs are the predominant driver of westward extensions.

1 Introduction

The Western Pacific subtropical high (WPSH) is an important driver of weather and climate variability over the Western North Pacific (WNP) region. The WPSH's variability is key in the prediction of boreal summer rainfall variability across the Indo-Pacific region, including East Asian monsoon rainfall (B. Wang et al., 2013; Guan et al., 2019), Indian summer rainfall (Chaluvadi et al., 2021), and tropical cyclone (TC) activity (B. Wang et al., 2013; Camp et al., 2018; Q. Wu et al., 2020; Johnson et al., 2022). Chang et al. (2000) observed that a westward extension of the WPSH's western edge is associated with increased monsoonal rainfall over East Asia, as an anomalous low-level westerly circulation channels moisture into the Yangtze River basin. B. Wang et al. (2013) showed that WPSH variability afforded considerable skill to WNP TC predictability, while Camp et al. (2018) demonstrated that TC predictability in models was strong due to a well-simulated WPSH. Studies such as Johnson et al. (2022) further showed that the WPSH's zonal variations or extensions play a substantial role in influencing seasonal WNP TC landfalling events.

Zonal extensions of the WPSH are characterized by anomalous geopotential heights over the WNP, along the WPSH's western edge, and strong easterly flow along the southern edge. Their interannual variability is strongly influenced by both local and remote sea surface temperature (SST) forcing (Lu, 2001; Lu & Dong, 2001; Dong et al., 2017; Guan et al., 2019). Known local SST forcings include the Pacific warm pool region (Lu, 2001; Lu & Dong, 2001), while the tropical Indian Ocean (TIO) (Xie et al., 2009, 2016; Kosaka et al., 2013; He & Zhou, 2015; Qian & Shi, 2017), the central (CP) and eastern Pacific (EP) regions (B. Wu et al., 2010; B. Wang et al., 2013; H. Li et al., 2020) have been identified as key remote forcings of WPSH variability. Alternatively, North Atlantic (ATL) SST variability may play a remote role in intensifying the WPSH and forcing WPSH meridional extensions (T. Li et al., 2017; Feng & Chen, 2021). The differential diabatic heating related to monsoons and the land-sea contrast is also important (Rodwell & Hoskins, 2001; Liu et al., 2004). Seager et al. (2003) suggested that the air-sea interaction and SST asymmetry amplify the circulation responses to monsoonal forcing. Furthermore, they showed that the global subtropical highs (STHs) reach their peak in the summer due to the strengthening of the west-east positive-negative SST asymmetry across each basin. Both B. Wang et al. (2013) and Kosaka et al. (2013) later showed that the leading modes of WPSH variability were supported by distinct modes of underlying zonal SST gradients.

A number of studies have shown that the WPSH has diverse responses to varying regional SST forcing within the underlying large-scale SST pattern. Many have shown that colder equatorial CP and EP SSTs enhance the WPSH and thus promote a stronger westward extension (B. Wu et al., 2010; Yuan & Yan, 2013; Z. Chen et al., 2016, 2017; M. Chen et al., 2019). M. Chen et al. (2019) found that differences in the preceding year's El Niño warming pattern resulted in varying WPSH development and intensification by different mechanisms. Jong et al. (2020) showed that summers with a transitional La Niña produced a stronger WNP anticyclone than La Niña-persisting summers. More recently, (Jiang et al., 2023) examined the diversity in WPSH response among seasons characterized by fast-decay El Niño events and showed that the WPSH's westward extensions were sensitive to SST differences. Faster El Niño decay rates resulted in the La Niña cold tongue reaching longitudes east of 160^{o}E during June-August. The La Niña's cold anomalies promoted subsidence over the WNP and anomalous anticyclonic flow. Slower decay rates resulted in lingering El Niño-associated warming that promoted convection and cyclonic flow over the WNP.

Atlantic (ATL) warming also plays a role in the WPSH's varying response during La Niña-developing summers (Hong et al., 2014, 2015; Zuo et al., 2019; Feng et al., 2020; Feng & Chen, 2021). But, many of the aforementioned studies have assessed the relative contributions of local and remote SST forcing to differences in WPSH response. Very few have examined the relative roles of tropical Indian Ocean, Pacific and Atlantic SST forcing in SST patterns that produce very similar responses in the WPSH. B. Wang et al. (2013) earlier demonstrated that the first two leading modes of WPSH variability, producing similar WPSH intensity, were driven by different atmosphere-ocean mechanisms. The first leading mode was characterized by a tropical Indian Ocean-WNP inter-basin zonal SST gradient. The second leading mode was characterized by an intra-basin warm WNP-cool CP and EP. In this study, we explore the relative contribution of regional SST forcing by comparing two large-scale SST patterns that produce very similar WPSH response. Here, we define inter-basin forcing as the remote impact of an external ocean to the atmospheric climate over the Pacific basin, while we use the term intra-basin to describe the impact of the local Pacific SSTs on the Pacific atmosphere.

While some of our conclusions are very similar to Jiang et al. (2023). We additionally show that similar changes in El Niño decay rate can also assess whether the underlying mechanism is inter-basin or intra-basin in nature. We explore the characteristic SST gradient pattern associated with the WPSH's westward extensions and compare the contribution of both inter-basin and intra-basin SST forcings to the WPSH's zonal variability. We compare whether the WPSH extensions are responding to single-region anomaly SST forcings (e.g. TIO and ATL SSTs) or SST gradient forcings. Additionally, we compare two similar large-scale SST patterns and assess how and why they provoke different atmospheric responses over the WNP, and assess the contributions from both local and remote SST forcings in each case. The questions we address in this paper are outlined as follows:

1. Can a comparable westward extension of the STH be forced by inter-basin and intra-basin SST drivers?
2. Which regional SST differences promote an inter-basin versus intra-basin mechanism?
3. How do the roles of the tropical Indian Ocean SSTs, equatorial central and eastern Pacific SSTs, and North Atlantic Ocean SSTs vary in an inter-basin versus intra-basin SST forcing?

The paper is outlined as follows. In section 2, we describe the data, methods, and experimental setup. Section 3 provides an observational analysis of the two similar SST patterns and their impact on the WPSH and its westward extensions. Section 4 outlines the results of our SST forcing experiments. Section 5 gives the discussion and conclusions.

2 Data and Methods

2.1 Data

Monthly variable fields are sourced from the ECMWF fifth generation reanalysis (ERA5) dataset (Hersbach et al., 2020). The ERA5 reanalysis dataset has a horizontal grid resolution of 31 km with 137 vertical levels, and provides data from 1 January 1940 to the present. Variables with a 0.25^ox0.25^o grid resolution were obtained from the Copernicus Climate Data Store (`https://cds.climate.copernicus.eu/cdsapp#!/home`) and are as follows: 850-hPa geopotential heights (Z850), 250-hPa, and 850-hPa zonal and meridional winds (UV250, UV850), and sea surface temperatures (SSTs). We analyze these fields over the time period 1979-2019. Anomalies calculated from these fields are relative to the 1979-2019 mean climatology. Note that our anomaly fields have not been detrended. In Section 3, we use the reanalysis variable fields to examine and characterize anomaly composites associated with the WPSH's extensions.

The WPSH's intensity and westward extensions are determined using the Z850 anomaly field. There are a variety of ways in which WPSH variability may be defined. Common indices used are calculated with geopotential height anomalies at 850-hPa (B. Wang et al., 2013; Camp et al., 2018) and 500-hPa (Zhou et al., 2009; Qian & Shi, 2017; H. Li et al., 2020). Less commonly used indices include 850-hPa relative vorticity (Kosaka et al., 2013; X. Wang et al., 2021). Following B. Wang et al. (2013), Camp et al. (2018), and Johnson et al. (2022), we define the WPSH intensity using 850-hPa geopotential height anomalies averaged over the tropical WNP region (10^o-30^oN, 100^oE-180^o). We also define the westward extension index (WEI) as the most westward longitude reached along the 1510-m contour within the WNP region. Under warming, positive geopotential height anomalies spread across the WNP due to atmospheric expansion, giving the illusion that the Pacific STH extends westward when measured by the spatial extent of a given height. Dong and He (2020) and H. Li et al. (2020) use similar methods to characterize the WPSH's zonal extensions in the 500-hPa height fields. The SST fields are used to calculate monthly standardized anomalies for the tropical Indian Ocean (TIO, 30^oS-30^oN, 40^o-120^oE), WNP, tropical North Atlantic (0^o-20^oN, 100^oW-0^o) and El Niño Southern Oscillation (ENSO) SST variability. The conventional Niño-3.4 region has been extended to 160^oE to better capture non-linear seasonal cold-tongue SST variations in the Central Pacific and equatorial eastern Pacific, as proposed by Williams and Patricola (2018). Therefore, the acronym ENSO is used hereafter to refer to the deep tropical equatorial Pacific SST anomalies between 10^oS-10^oN and 160^oE-120^oW.

2.2 CAM6 and Experiment Setup

We simulate the response of the WPSH using the atmosphere-only component of Community Earth System Model version 2.2.0 (CESM2). The Community Atmosphere Model version

6 (CAM6) uses a 0.9^{o}x1.25^o horizontal resolution and 32 vertical levels with a Finite Volume (FV) dynamical core (Danabasoglu et al., 2020). Our experimental setup consists of atmosphere-only (AMIP) simulations using the F2000CLIMO configuration driven by a historical 12-monthly SST climatology representative of present-day climate, and is run with active atmosphere (CAM6) and land (CLM5) components. A detailed description of F2000CLIMO and other CESM2 run configurations can be found at `https://www.cesm.ucar.edu/models/cesm2/config/compsets.html`. The F2000CLIMO compset provides a simplified experimental setup that directly tests the general circulation's response to recurring seasonal SST changes independent of year-to-year SST variability.

To examine how SSTs force the WPSH, we run the F2000CLIMO component set that forces CAM6 with a 12-month prescribed SST climatology. The control experiment (CTRL) is taken to be the 1979-2019, calculated from the ERA5 reanalysis dataset. Note that the ERA5 SST fields are regridded to the CAM6 grid resolution (1.9^{o}x2.5^o), and are linearly interpolated to fill in masked land values prior to running the simulations. The first SST composite (COMP1) comprise years 1980, 1995, 1998, 2003, and 2010, in which the June-August WPSH is most enhanced and the 1510-gph contour is most westward extended. The second SST forcing (COMP2) is composited from years 1980, 1983, 1998, 1999, and 2010. While there is considerable overlap between the two sets of years, the addition of 1983 and 1999 in COMP2 results in a larger spread of negative SST anomalies across the central and eastern Pacific regions without significantly changing the magnitude of the La Niña (Figure 2). This partial overlap is by design. As we will show below, somewhat subtle differences in SST anomaly patterns between the two composites result in markedly different outcomes for the drivers of the westward extension. In practice, experiments for these two distinct composites were initially done by accident, but serendipitously, they yielded an interesting contrast in behavior that became the focus of this work. Then, the COMP1 and COMP2 SST patterns are quadrupled in magnitude (*4xWEST*) to enhance the westward extension signal in the simulations relative to the *CTRL* simulation. The simulations are allowed to run for 6 years. The first year is thrown out to account for model initialization, and the atmospheric response is averaged over years 2-6. We ran initial experiments out to years 6, 11, 16, and 31 and found no significant changes from the simulated westward extent averaged over years 2-6.

Note that, since the simulations are driven only by the prescribed 12-month SST climatology, the simulations are not forced by SST variations from preceding years, and therefore, doesn't take into account lagged air-ocean impacts, for example, ENSO's and TIO's lagged relationships from the year prior (M. Chen et al., 2019). Similarly, the WPSH is also a result of coupled air-sea interactions (T. Li et al., 2017). The study to follow only examines the atmospheric response to the prescribed SSTs. In the sections to follow, we compare the WPSH's response across the *4xWEST* simulations.

To test which specific regional SST anomalies generate an enhanced WPSH comparable to the original *4xWEST* simulations, we run a set of experiments in which we progressively constrain the region of SST anomalies included in the *4xWEST* forcing. We note that, when forced with the WEST SST patterns, CAM6 produces a weaker westward extension relative to the *CTRL* experiment (not shown). This suggests that tropical convection in CAM6 may be less effective in generating subtropical high responses, likely due to differences in the diabatic heating profiles (R. Chen et al., 2022). Therefore, the *4xWEST* forcing is chosen to enhance the simulated WPSH's westward extension relative to the control simulation, which produces a WPSH westward extension of 134.9^{o}E and 128.7^{o}E for COMP1 and COMP2, respectively. We illustrate this contribution by comparing the difference in the 850-hPa geopotential heights between the spatially adjusted experiments and the CTRL experiment. Figure 1 illustrates the forcing domains for the experiments listed in Table 1.

Table 1 lists and organizes all simulations analyzed in this study into four experimental sets. Excluding the *CTRL* and *4xWEST* experiments, all other experiments comprise constraining SST anomalies to select domains and zeroing SST forcing elsewhere. Experimental set 1 examines the individual contributions of the tropical Indian Ocean (TIO), Pacific Ocean (PAC), and Atlantic Ocean (ATL) basin SST anomalies to the global COMP1 and COMP2 *4xWEST* forcings. These three basins have previously been shown to play substantial roles in the development and maintenance of the WPSH (Lu & Dong, 2001; B. Wu et al., 2010; W. Li et al., 2012; T. Li et al., 2017). In the following sections, we will show that these basin contributions are not comparable between COMP1 and COMP2.

In experiment set 2, SSTs are constrained to the North Pacific basin (as defined in Table 1) and examines whether Pacific SST magnitude, and consequently the strength of the zonal SST gradient across the Pacific, drives the stark difference in response between the COMP1 *PAC* and COMP2 *PAC* forcings. For these experiments, the magnitude of negative *PAC* SST anomalies (-SSTA) for COMP1 is doubled (*PACx2*) and then tripled (*PACx3*) to enhance the original COMP1 *PAC* zonal SST gradient. Note that the *PACx2* and *PACx3* are conducted only for COMP1's *PAC* forcing.

Experiment sets 3 and 4 examine the individual contributions of intra-basin SST forcing by constraining SSTs to the tropical (*TBAND*) and extratropical (*EXTBAND*) domains in the North Pacific and Atlantic basins, respectively. The TBAND and EXTBAND domains were chosen based on the distribution of COMP1 minus COMP2 SST differences (Figure 3c). Additionally, Jiang et al. (2023) showed that the subtropical and extratropical regions may provide additional forcing along with well-known forcing from the Pacific and Atlantic tropical belts. Therefore, we define *PAC TBAND* and *PAC EXTBAND* intra-basin SST forcings for the North Pacific basin, and *ATL TBAND* and *ATL EXTBAND* SST forcings for the Atlantic basin.

For all experiments, the change in WEI is taken relative to the mean control. Statistical significance is determined via sample mean bootstrapping for a sample size of N=5 (see Figure S1). Therefore, extensions westward of 151.4^{o}E are considered statistically significant at the 95% level for *4xWEST* simulations. Note also that no smoothing was applied to the edges of the SST patterns. A comparison of the SST-forced simulations with smoothing versus no smoothing achieved similar results (not shown). Finally, we acknowledge that the WPSH is maintained by coupled atmosphere-ocean interactions (Seager et al., 2003). By using atmosphere-only simulations, our paper focuses only on the atmosphere's response to the SST pattern.

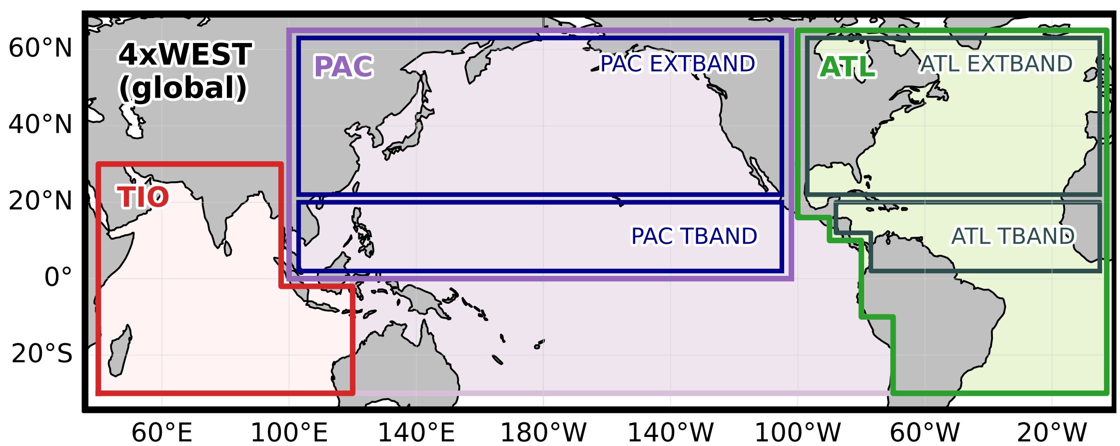

Figure 1. Outline of the main SST pattern forcing domains. The main domains include the tropical Indian Ocean (TIO, red), the North Pacific Ocean basin (PAC, purple), and the Atlantic Ocean basin (ATL, green).

Table 1. List of sea surface temperature forcing experiment sets, regional domains used, and brief descriptions of each experiment.

Experiment Set	Experiment Name	Description
1	1979-2019 Control (CTRL)	–
	4xWEST (Global)	–
	4xWEST minus ATL	ATL basin SSTs zeroed.
	4xWEST minus ATL,TIO	Both ATL and TIO basin SSTs zeroed.
2	North Pacific basin (PAC)	COMP1, COMP2 experiments.
	PACx2	COMP1 PAC -SSTA multiplied by 2, with lingering El Niño +SSTA changed to -SSTA.
	PACx3	As for PACx2, but -SSTA multiplied by 3.
3	PAC TBAND	0^o-20^oN, 100^oE-160^oW
	PAC EXTBAND	20^o-60^oN, 100^oE-160^oW
4	ATL only	North and South Atlantic basins
	ATL TBAND	0^o-20^oN, 100^oW-0^o
	ATL EXTBAND	20^o-60^oN, 100^oW-0^o

3 Two similar SST patterns belie two different SST forcing mechanisms

The COMP1 and COMP2 SST patterns have very similar SST patterns with only minor differences in SST and Z850 anomalies. Figure 1 shows the SST and Z850 anomaly fields associated with each season composite and the COMP1 minus COMP2 composite difference. As is characteristic of summer seasons in which a strong westward extension of the Pacific subtropical high has occurred, the underlying SST anomaly pattern consists of positive SST anomalies in the tropical Indian Ocean and western North Pacific, negative SST anomalies in the central Pacific, a decaying El Niño or developing La Niña within the equatorial eastern Pacific, and positive tropical North Atlantic SSTs.

Figure 2c indicate that most of the differences in SSTs between COMP1 and COMP2 lie in the tropical and subtropical central and eastern Pacific, and the subtropical/extratropical Atlantic regions. These differences are fairly small, ranging between -0.6^{o}C to +0.6^{o}C, and show no equivalent effect in the Z850 anomaly composite difference (Figure 2f). The two SST composites also show similarities in the monthly evolution of SSTs in key regions for WPSH development and maintenance. Figure 3a and 3b show the YR(-1) and YR(0) monthly mean standardized anomalies averaged over the TIO, extended ENSO domain (20^oS-20^oN, 160^oE-120^oW), WNP, and the TNA. COMP1's D(-1)JF El Niño event is slightly stronger than that of COMP2, but both composites indicate a comparable rate of decay of the winter El Niño. The June-August La Niña SST signal averages -0.66^{o}C for COMP1 and -0.78^{o}C for COMP2. See Figure S2 for monthly SST evolution for each year used to create the two SST composite patterns.

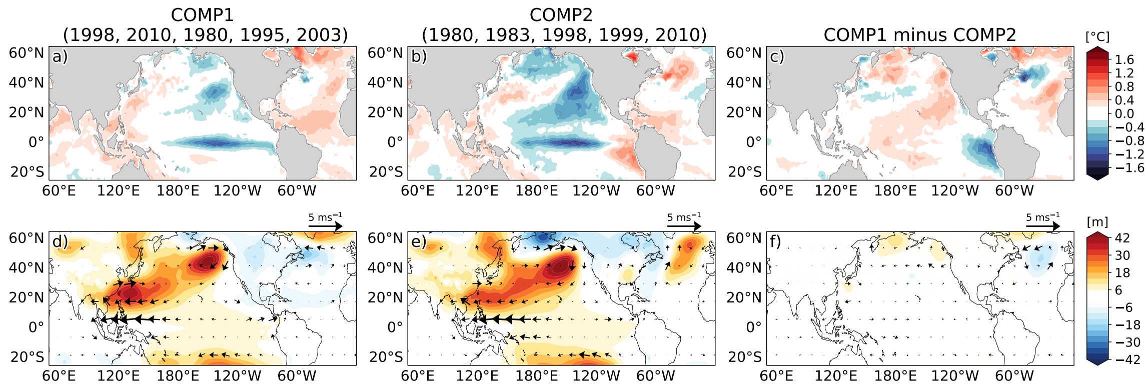

Figure 2. Composites and composite difference of June-August mean anomalous (a-c) SSTs, and (d-f) 850-hPa geopotential heights (shaded contours, m) with horizontal winds (quivers, m s^{-1}) for COMP1 (1998, 2010, 1980, 1995, and 2003) and COMP2 (1980, 1983, 1998, 1999, and 2010).

Figures 3c and 3d illustrate the monthly evolution of standardized SST anomalies averaged over the tropical band between 20^{o}S-20^{o}N. The figures indicate that both COMP1 and COMP2 reflect an eastern Pacific (EP) La Niña-type signal, and even have a similar seasonal development of La Niña, following from a strong winter EP El Niño from the preceding year (Figure 2). The key difference between the two composites lies in the decay of the winter El Niño. In COMP1, the eastward migration of central Pacific negative SST anomalies doesn't occur until around April-May. In contrast, for COMP2, this eastward migration begins the year before (not shown) and can be observed in months January-March. In consequence of the earlier decay of COMP2's winter El Niño, negative SSTs >0.5^{o}C develop earlier in the summer, and are shown to spread further west into the central Pacific region.

In the CAM6 simulations, COMP1 and COMP2 show comparably strong westward extensions. Figures 4a and 4b illustrate the atmospheric response in 850-hPa geopotential heights to the *4xWEST* global SST forcing for COMP1 (Figure 4a) and COMP2 (Figure 4b). COMP1 and COMP2 produce WEI changes of -17^o and -23^o, respectively, statistically significant at the 95% confidence level from the *CTRL*. The two SST patterns also produce anomalous anticyclones of similar intensity over the WNP (not shown). This result is consistent with our observational analysis (Figures 2 and 3) and shows that COMP1 and COMP2 have similar impacts on the WPSH.

Despite similar responses to global SST anomalies, experiments constraining SST anomalies to individual basins give very different results, suggesting different sources of forcing. The first experimental set examines the relative contributions of three key regions for westward extensions simulated by the *4xWEST* experiments: the *ATL*, *TIO*, and *PAC*. In Figures 4c and 4d illustrate the COMP1 and COMP2 *4xWEST minus ATL* experiments, respectively, that illustrate the impact of removing *ATL* SSTs from the global SST forcing pattern. Figures 4e and 4f show the result

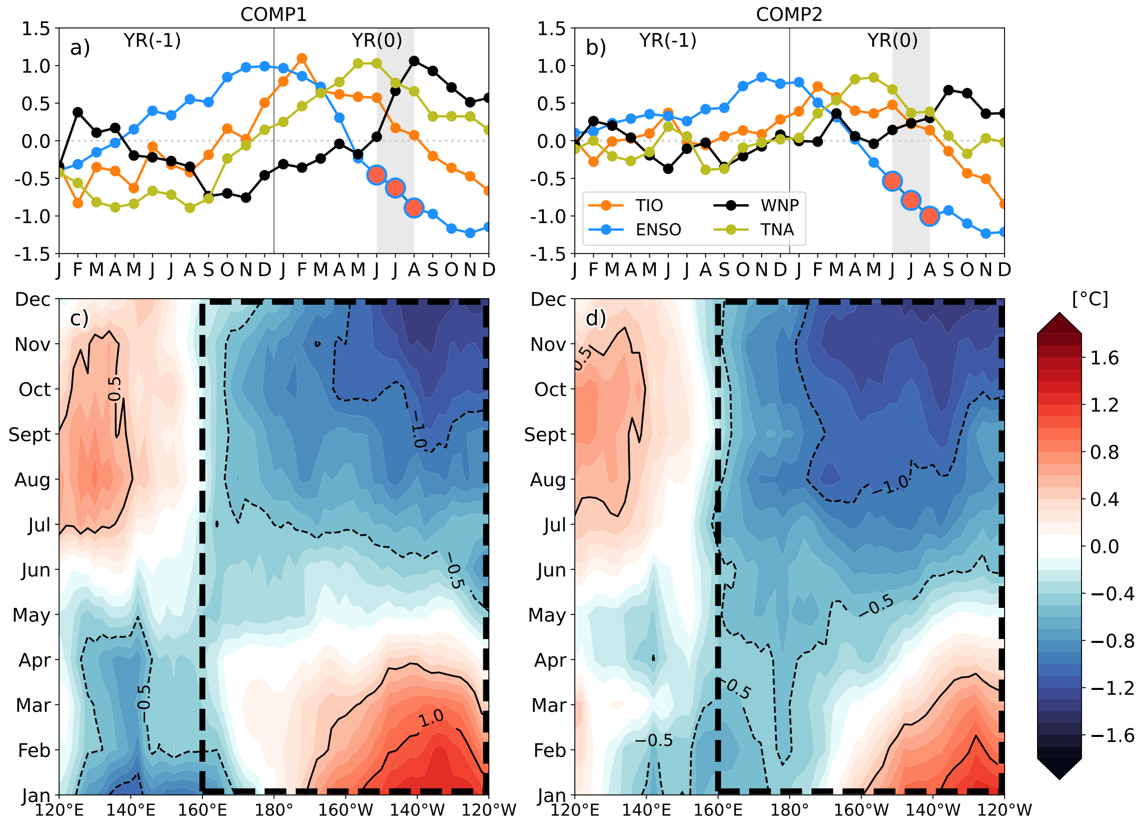

Figure 3. (a, b) Monthly mean standardized SSTs averaged over the TIO, WNP, equatorial eastern Pacific (ENSO), and the tropical North Atlantic (TNA) regions for the contemporaneous year (YR(0)) and the preceding year (YR(-1)). The YR(0) June-August (JJA) - which is the main focus of this study- is highlighted by the gray shading. ENSO values during JJA are highlighted by the large pink dots. (c, d) Longitude-time plot averaged over 20^oS-20^oN illustrates ENSO's monthly evolution during YR(0). Dashed box outlines the ENSO region, defined as 20^oS-20^oN and 160^oE-120^oW. The extended ENSO domain considers the longitudinal extent of the cold tongue anomalies (Williams & Patricola, 2018). The TNA region is defined as 0^o-20^oN, 100^oW-0^o.

of further removing *TIO* SSTs from the global SST forcing pattern, leaving just the *PAC* basins. Note that the westward extensions produced by COMP1 *4xWEST* falls off quickly once the ATL (and to a lesser extent, the *TIO*) is removed. In contrast, for the COMP2 *4xWEST* simulations, the *PAC* SSTs maintain the westward extension observed for its *4xWEST* simulation, with only a small change in WEI with the removal of *TIO*. This suggests that the COMP1 SST pattern forces westward extensions predominantly through inter-basin SST gradients while the COMP2 SST pattern forces westward extensions through intra-basin Pacific SST gradients.

The large-scale SST pattern's forcing of westward extensions can be viewed from the perspective of the zonal Pacific overturning atmospheric circulation. Figures 5a and 5b illustrate the meridional cross-section of the tropical atmospheric circulation averaged from 0^o-30^oN. Both COMP1

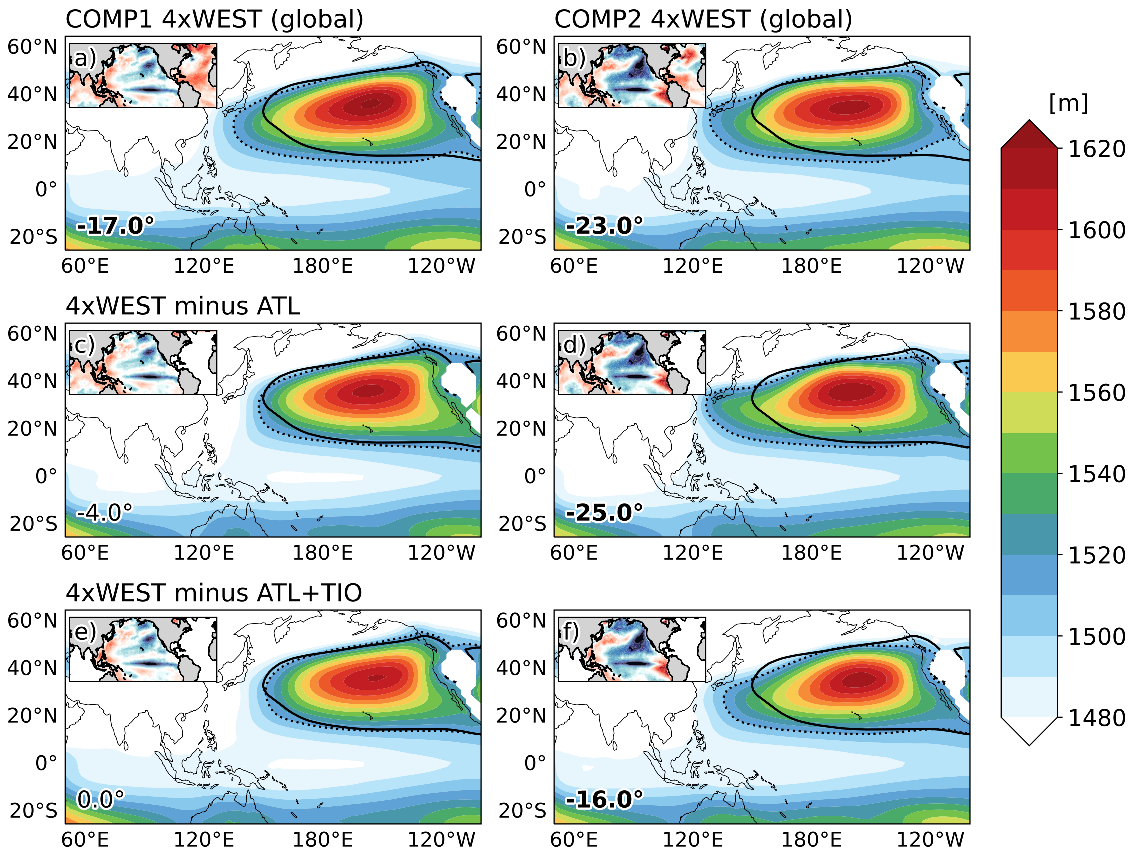

Figure 4. COMP1 versus COMP2 comparison of simulated 850-hPa geopotential heights in response to (a, b) *4xWEST*, (c, d) *4xWEST minus ATL*, (e, f) *4xWEST minus ATL+TIO* simulations. Inset plots showcase the respective SST forcing for each simulation. The solid black contour outlines the 1510-gph contour in *CTRL* simulation, while dashed contours outline the 1510-gph contour for the respective forcing simulations. The mean westward extent index (WEI) value produced by each experiment, expressed as the change relative to the *CTRL* WEI, is given in the bottom left corner of each subplot. Note that negative (positive) WEI changes indicate a westward extension (eastward retraction). WEI changes that are statistically significant at the 95% confidence level are highlighted in bold.

and COMP2 are characterized by strong subsidence over the central Pacific (the descending arm of the Walker Circulation) and ascent over the TIO and Atlantic regions. In the lower levels, the strong easterly flow associated with an enhanced WPSH and westward extension may be observed over the Indo-Pacifc/WNP region between 100^{o}E-180^o. As the ATL and TIO forcings are removed, the descending arm supporting the strong lower-level easterlies over the central Pacific collapses for COMP1 (Figures 5c, 5e), but remains intact for COMP2 (Figures 5d, 5f). Note that when SSTs are further constrained, the WNP proves to be the smallest region that a statistically significant westward extension in COMP2. Therefore, for COMP1, the combined effect of the Atlantic SSTs and the tropical Pacific-Indian Ocean/WNP SST gradient lead to a robust westward extension of the STH.

So, why are the relative contributions of regional SSTs so different between the COMP1 and COMP2 SST patterns? From Figure 1c, we identify and examine three key regions of SST differences stand out in Figure 1c that may explain the difference in model response, which we further explore using the atmosphere-only CAM6 global climate model: the tropical and subtropical central and eastern Pacific SSTs, extratropical Pacific SSTs, and the subtropical and extratropical Atlantic SSTs.

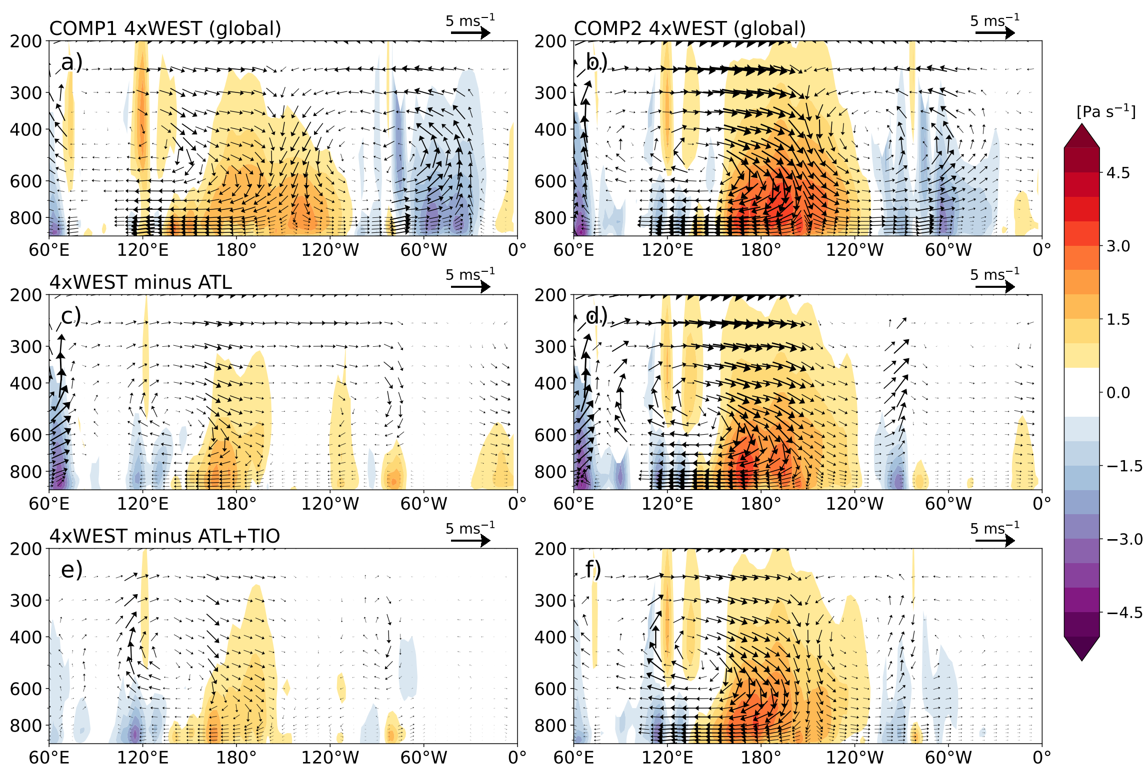

Figure 5. Meridionally-averaged longitude-pressure plots of vertical velocity anomalies (shading), with quivers representing the magnitude and direction of scaled vertical (x100) and zonal (x0.5) wind anomalies from the same experiments as Fig. 4. All plots are averaged over latitudes 0^o-20^{o}N.

4 Tropical Pacific intra-basin SST forcing of westward extensions can be suppressed by its extratropical SST forcing

In the previous section, we showed that the relative contributions from remote SSTs (inter-basin forcing) predominantly drive westward extensions in COMP1 simulations, while local Pacific SSTs (intra-basin forcing) are the predominant driver in COMP2 simulations. Jiang et al. (2023) observed that the *TIO* and *ATL* SSTs were strong drivers of westward extensions in seasons with faster El Niño decays. The atmospheric response to the COMP1 SST pattern reflects the importance of remote SSTs to its forcing mechanism and is consistent with Jiang et al. (2023)'s findings (Figures 5a, 5e, 5e). But COMP2 contradicts the profile for this mechanism, despite having a stronger zonal SST gradient in the equatorial North Pacific than COMP1 (see Figure S3a) with arguably similar El Niño decay rates (Figure 3). The results of this study and Jiang et al.'s results suggest that there is a big difference in the forcing impact between COMP1 and COMP2 Pacific basin SSTs. In the second experiment set, we test the differences between the COMP1 and COMP2 North Pacific SST forcing.

Figure 6 compares the simulated WPSH forced by North Pacific SST forcing (*PAC*) for COMP1 (Figure 6a,6e) and COMP2 (Figure 6d,6h). Negative SST anomalies in COMP1's *PAC* forcing were doubled (*PACx2* in Figures 6b, 6f) and then tripled (*PACx3* in Figures 6c, 6g) to assess the impact of cold central Pacific anomalies on COMP1's forcing. Increasing the magnitude of the CP and EP negative anomalies results in only a slight improvement in westward extension (Figure 6a, 6b), suggesting that the distribution of negative CP and EP SST anomalies is one key reason for the strong westward extension forced by COMP2's *PAC* experiment, presumably by increasing the zonal SST gradient across the Pacific basin. These results are consistent with previous studies that show the state and transition of the summer La Niña can play a major role in forcing the atmospheric response over the WNP (Jong et al., 2020; H. Li et al., 2020; Jiang et al., 2023).

Hence, the distribution and strength of the tropical CP and EP negative SST anomalies alone do not explain the stronger westward extension and anomalous anticyclone produced for the COMP2 *PAC* forcing (Figures 6d and 6h). There remains no significant westward shift in the presence of a substantial zonal SST gradient in the tropical Pacific (for an SST profile, see Figure S3b). Therefore, in experimental set 3, we examine the contributions of SSTs in the Pacific tropical band (*TBAND*), between 0^o-20^oN, and subtropical and extratropical domain (*EXTBAND*) to the JJA westward extensions.

The SST anomalies from the Pacific tropical band alone produces a comparable westward extension in COMP1 and COMP2 (*PAC TBAND*; Figures 7a vs. 7b). Similarly, the *PAC EXTBAND* forcings for both COMP1 and COMP2 produce negative Z850 anomalies and an anomalous cyclone over the WNP. However, the COMP1 *PAC EXTBAND* forces a stronger cyclonic flow, likely from the broader spread of positive SST anomalies along the western boundary. Similar observations have

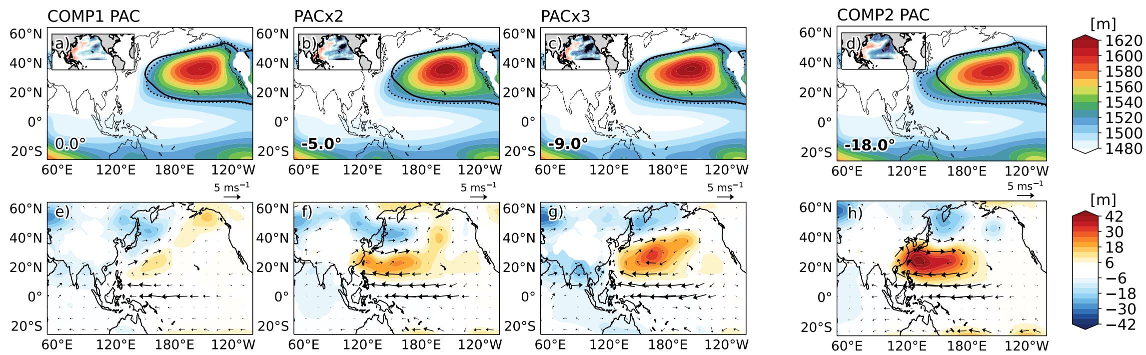

Figure 6. Simulation response in 850-hPa geopotential heights (top panels) and height anomalies relative to *CTRL* (bottom panels) to COMP1's (a, e) *PAC*, (b, f) *PACx2*, and (c, g) *PACx3*, compared to (d, h) COMP2's *PAC* experiment.

been made by Jiang et al. (2023). COMP1's *PAC EXTBAND* similarly produces an anomalous WNP cyclone, but the strength of this cyclone is curtailed by anomalous anticyclonic flow further north. Figure 7e shows the mean Z850 anomaly over the WNP for the *PAC TBAND* and *PAC EXTBAND*, and the net *TBAND+EXTBAND* forcing for both COMP1 and COMP2. For COMP1, the net *PAC* forcing reflects the suppression of the *PAC TBAND* forcing by *PAC EXTBAND* and produces similar Z850 anomalies as those forced by COMP1 *PAC* (Figure 5e). For COMP2, the relatively stronger forcing by COMP2 *TBAND* is enough to withstand forcing from its *EXTBAND*. Therefore, a key difference in the inter-basin versus intra-basin forcing of COMP1 and COMP2 stems from the difference in net Pacific forcing.

5 Remote Atlantic SST forcing drives westward extensions when the local net Pacific forcing is weak

From experimental sets 2 and 3, we have shown that the net contributions between the *PAC* and *ATL* basin SSTs may vary depending on the net PAC forcing. When *PAC TBAND* is much stronger than *PAC EXTBAND*, the westward extensions are driven predominantly by intra-basin *PAC* SST forcing. When the *PAC TBAND* is suppressed by *PAC EXTBAND*, the *ATL* and *TIO* SSTs (and hence inter-basin SSTs) predominantly force the westward extensions. Since the *TIO* forcing for COMP1 and COMP2 are identical (see Figure S4), the remaining SST difference lies with the *ATL*. So, are the *ATL* forcings significantly different between COMP1 and COMP2?

The results of the fourth experimental set show that the *ATL* SST forcing has comparable impacts on the WPSH's westward extension for both COMP1 and COMP2. Despite a clear difference between the COMP1 and COMP2 ATL SST patterns, both forcings produce a WEI change of -15^{o}E (Figures 8a, 8b). The key mechanism underlying the Atlantic forcing of WNP westward extensions

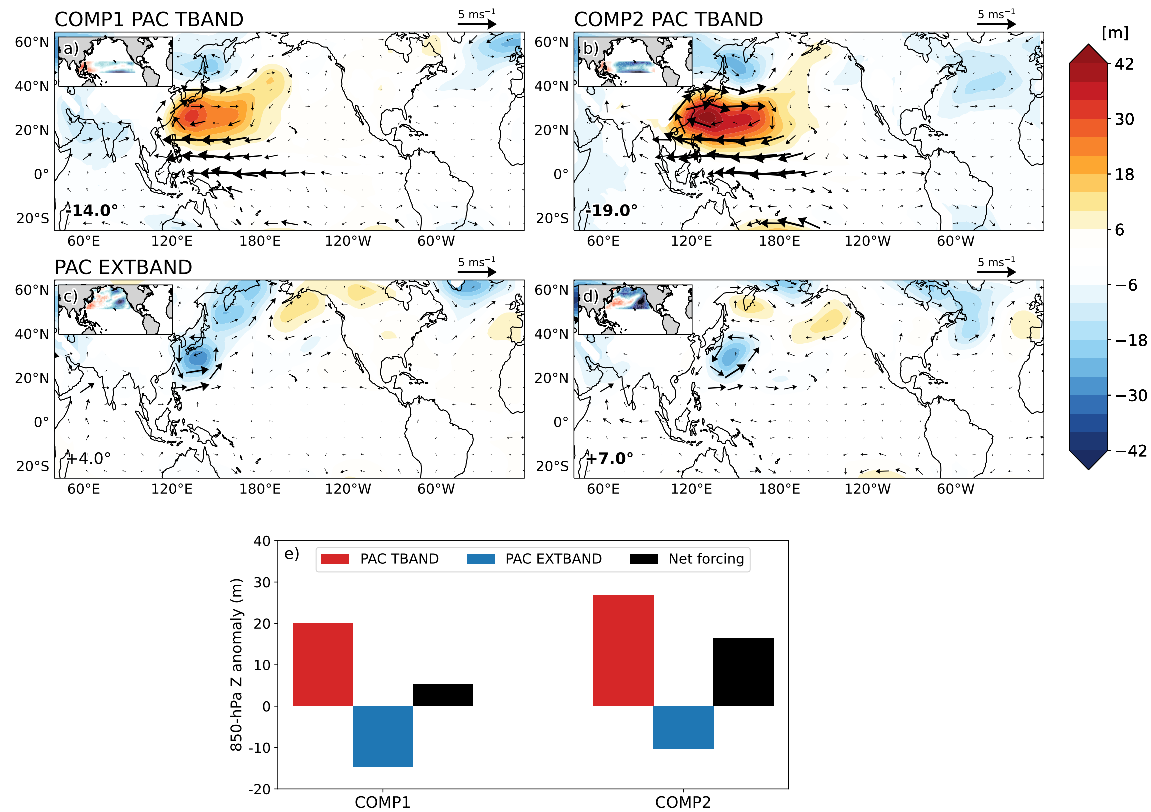

Figure 7. COMP1 versus COMP2 comparison of simulated 850-hPa geopotential height anomaly response to the forcing domains (a, b) *PAC TBAND*, and (c, d) *PAC EXTBAND*. e) Mean 850-hPa geopotential anomaly averaged over 10^o-30^oN and 100^oE-180^o for COMP1's and COMP2's Pacific *TBAND* and *EXTBAND* simulations.

comprises the forcing of an anomalous low-level cyclonic circulation, strong westerlies, and negative Z850 anomalies over the western North Atlantic. This atmospheric response likely spurs strong ascent (see Figure 5a) which in turn forces strong subsidence over the WNP. When the *ATL* forcing is divided into the *ATL TBAND* and *ATL EXTBAND* domains, the *ATL TBAND* proves to be the key contributor to the larger *ATL* pattern (Figures 8c, 8d), consistent with studies that show that the tropical Atlantic SSTs can substantially force the WNP anomalous cyclone and, consequently, westward extensions (Lu & Dong, 2005; Hong et al., 2014; Zuo et al., 2019). The COMP2 *ATL TBAND* produces a slightly weaker extension compared to COMP1. Since the *ATL EXTBAND* forcings show no significant westward extensions, the difference in the *ATL TBAND* forcings is attributed to the widespread positive tropical North Atlantic SST anomalies in COMP1 that may drive a stronger response over the western North Atlantic.

Unlike the net Pacific forcing of westward extensions, the net forcing from COMP2's Pacific (-17^{o}E) and Atlantic (-15^{o}E) SSTs do not add linearly to recover its original 4xWEST forcing (-23^{o}E) (Figures 4b, 6d, 8b). The strong relative contributions from both the Pacific and Atlantic basins clearly explain why COMP2 provides a stronger westward extension than COMP1. But, if the two basins provide comparable impacts on the WPSH's westward extension, why does one basin show a stronger forcing over the other? We suggest that, in contemporaneous forcing experiments, the location of the forcing relative to the subsidence region matters. If local and remote SST forcings are similar (as in the case of COMP2), the westward extensions are more likely to be driven by SST anomalies in close proximity to the WPSH. Idealized experiments (not shown) show that the westward extensions are sensitive to zonal shifts of the zonal SST gradient. Studies such as Jiang et al. (2023) also imply this sensitivity, as cases in which the westward reach of equatorial Pacific cold SST anomalies (and thus stronger zonal SST gradient) also produce a stronger forcing of WPSH westward extensions.

6 Discussion and Conclusion

Many studies have highlighted the importance of SSTs in driving the WPSH's zonal variability. Many have concluded that the tropical Indian and equatorial eastern Pacific SST variability are key drivers of the WPSH's zonal extensions (B. Wang et al., 2013; H. Li et al., 2020). In this study, we examined which SSTs across the Indian and Pacific Oceans matter for the westward extensions by progressively constraining the SST forcing within atmosphere-only CESM2 model simulations. The simulated WPSH's response to our forcing simulations is outlined in Table 2, and our key conclusions are summarized as follows:

1. In comparing two very similar SST patterns (COMP1 and COMP2), we find that the large-scale zonal inter-basin SST gradient that characterizes decaying El Niño and developing

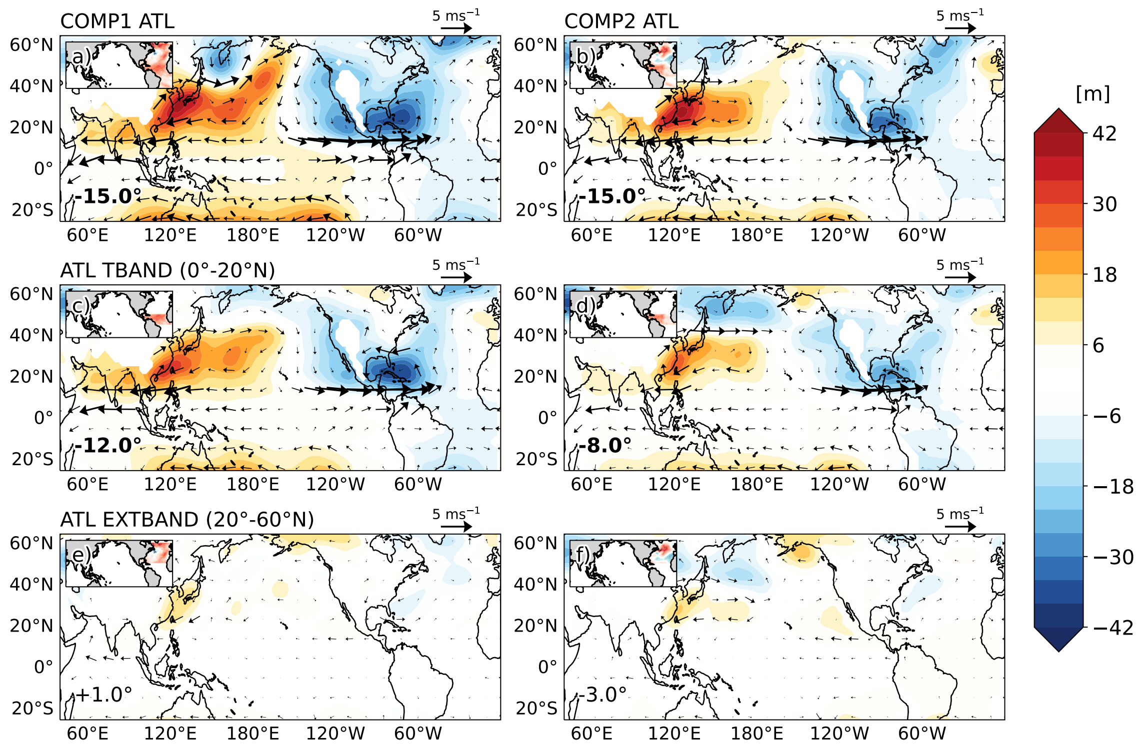

Figure 8. COMP1 versus COMP2 comparison of simulation response to experiments (a, b) *ATL* only, (c, d) *ATL TBAND*, and (e, f) *ATL EXTBAND*.

La Niña summers, is not always the predominant driver of the WPSH's westward extensions. While COMP1 and COMP2 force comparable westward extensions, the relative contributions from remote SSTs (inter-basin forcing) predominantly drive westward extensions in COMP1 simulations, while local Pacific SSTs (intra-basin forcing) are the predominant driver in COMP2 simulations.

2. One key reason for the difference in net contributions is likely due to differences in state of the summer El Niño decay. The meridional spread and magnitude of central Pacific and eastern Pacific negative SST anomalies, and even the presence of lingering El Niño-related positive SST anomalies, weakens the Pacific zonal SST gradient in COMP1. However, this only partially explains the inter-basin SST forcing of westward extensions by the COMP1 SST pattern. The second key reason is that the SSTs north of 20^{o}N tends to force anomalous cyclonic circulation over the WNP. In COMP1, the Pacific *TBAND* forcing of westward extensions is completely suppressed by its *PAC EXTBAND* forcing, while COMP2's Pacific *TBAND* forcing is strong enough to withstand suppression from it's *PAC EXTBAND* forcing.
3. When the net *PAC* forcing is weak, the Atlantic SST forcing drives the westward extensions. The COMP1 and COMP2 SST patterns show that a warm *ATL TBAND* forces significant westward extensions. Note that the *PAC* and *ATL* forcing simulations show comparable forc-

Table 2. Summary of the mean westward extension for each experiment, expressed as a change from the CTRL simulation. Negative (positive) values indicate a westward extension (eastward retraction). As with prior figures, values highlighted in bold represent statistical significance at the 95% confidence level.

Experiment	COMP1 WEI	COMP2 WEI
4xWEST (Global)	**-17^o**	**-23^o**
4xWEST minus ATL	-4^o	**-25^o**
4xWEST minus ATL,TIO	0^o	**-16^o**
PAC	0^o	**-18^o**
PACx2	**-5^o**	–
PACx3	**-9^o**	–
PAC TBAND	**-14^o**	**-19^o**
PAC EXTBAND	0^o	-2^o
ATL only	**-15^o**	**-15^o**
ATL TBAND	**-12^o**	**-8^o**
ATL EXTBAND	+1^o	-3^o

ing of westward extensions, but do not contribute in equal portions to the original *4xWEST* forcing, particularly for COMP2 (see Figure S5). Instead, they may alternate the driving role of the Walker Circulation, depending on the net Pacific SST forcing, as illustrated by Figure 4. This suggests that the relative contributions of the tropical Indian Ocean, Pacific, and Atlantic basins may be non-linear in nature. This may not be entirely surprising considering that the individual basins can have considerable influence on each other (Hoerling et al., 2001; Chikamoto et al., 2020; Hu & Fedorov, 2020; Park et al., 2023).

The results of this paper also has implications for understanding WPSH westward extension variability and the sources of SST forcing. Jiang et al. (2023) showed that the westward extensions are sensitive to the rate of development of ENSO and thus the strength of the tropical zonal SST gradient with negative impacts from subtropical Pacific SSTs. Our study further shows that these characteristics may also determine whether the westward extensions are driven predominantly by inter-basin Atlantic SST forcing versus intra-basin Pacific SST forcing. Additionally, Hong et al. (2014) observed that the influence of tropical Atlantic warming on the WPSH has strengthened in recent over recent decades. Seager et al. (2019) observed that precipitation trends favor increased precipitation over the western Pacific with decreased precipitation over the central Pacific, indicating a strengthening of the zonal equatorial Pacific SST gradient. Further work will examine the contributions of a warmer tropical Atlantic and strengthened equatorial Pacific SST gradient to future variability and thus predictability of WPSH zonal extensions. Tropical Atlantic warming has been shown to induce a La Niña-like pattern (McGregor et al., 2014; Chikamoto et al., 2020; Fosu et al., 2020; Park et al., 2023). It could be possible in a fully-coupled framework, that remote tropical

Atlantic warming and the Atlantic's forced development of a La Niña may promote WPSH intensification. In addition, the pattern of Atlantic warming in COMP1 is similar to the positive phase of the Atlantic Multidecadal Variability (AMV) and provides further motivation for understanding of the remote impacts of the Atlantic Ocean on WPSH development.

7 Open Research

The SST forcing files and model builds used in this analysis (Jones et al., 2023) are available at the Zenodo repository `https://doi.org/10.5281/zenodo.10127842`. The ERA5 reanalysis dataset (Hersbach et al., 2017) is publicly available through the Copernicus Climate Data Store (`https://cds.climate.copernicus.eu`). The previous and current versions of the CESM2 global climate model (UCAR, 2018) is freely available to the public and may be found at `https://www.cesm.ucar.edu/models/cesm2/`.

Acknowledgments

This research was supported by the National Science Foundation (NSF) Faculty Early-Career Development Program (CAREER) Award 1945113. We would like to acknowledge high-performance computing support from Cheyenne (doi:10.5065/D6RX99HX) provided by NCAR's Computational and Information Systems Laboratory, sponsored by the NSF. Finally, we thank all the scientists, software engineers, and administrators who contributed to the development of CESM2. We also thank the Editor and Reviewers for the helpful comments and suggestions that helped to improve the quality of our publication.

References

Camp, J., Scaife, A. A., & Heming, J. (2018). Predictability of the 2017 North Atlantic hurricane season. *Atmospheric Science Letters*, *19*(5), e813. https://doi.org/10.1002/asl.813.

Chaluvadi, R., Varikoden, H., Mujumdar, M., & Ingle, S. (2021). Variability of West Pacific subtropical high and its potential importance to the Indian summer monsoon rainfall. *International Journal of Climatology*, *41*(7), 4047–4060. https://doi.org/10.1002/joc.7057.

Chang, C., Zhang, Y., & Li, T. (2000). Interannual and interdecadal variations of the East Asian summer monsoon and tropical Pacific SSTs. Part I: Roles of the subtropical ridge. *Journal of Climate*, *13*(24), 4310–4325. https://doi.org/10.1175/1520-0442(2000)013%3C4310:IAIVOT%3E2.0.CO;2.

Chen, M., Yu, J.-Y., Wang, X., & Jiang, W. (2019). The changing impact mechanisms of a diverse El Niño on the western Pacific subtropical high. *Geophysical Research Letters*, *46*(2), 953–962. https://doi.org/10.1029/2018GL081131.

Chen, R., Simpson, I. R., Deser, C., Wang, B., & Du, Y. (2022). Mechanisms behind the springtime north pacific ENSO teleconnection bias in climate models. *Journal of Climate*, *35*(23), 4091–4110. https://doi.org/10.1175/JCLI-D-22-0304.1.

Chen, Z., Wen, Z., Wu, R., & Du, Y. (2017). Roles of tropical SST anomalies in modulating the western north Pacific anomalous cyclone during strong La Nicaying years. *Climate Dynamics*, *49*, 633–647. https://doi.org/10.1007/s00382-016-3364-4.

Chen, Z., Wen, Z., Wu, R., Lin, X., & Wang, J. (2016). Relative importance of tropical SST anomalies in maintaining the western North Pacific anomalous anticyclone during El Niño to La Niña transition years. *Climate Dynamics*, *46*, 1027–1041. https://doi.org/10.1007/s00382-015-2630-1.

Chikamoto, Y., Johnson, Z. F., Wang, S.-Y. S., McPhaden, M. J., & Mochizuki, T. (2020). El Niño?Southern Oscillation Evolution Modulated by Atlantic Forcing. *Journal of Geophysical Research: Oceans*, *125*(8), e2020JC016318. https://doi.org/10.1029/2020JC016318.

Danabasoglu, G., Lamarque, J.-F., Bacmeister, J., Bailey, D., DuVivier, A., Edwards, J., ... others (2020). The community earth system model version 2 (CESM2). *Journal of Advances in Modeling Earth Systems*, *12*(2), e2019MS001916. https://doi.org/10.1029/2019MS001916.

Dong, X., & He, C. (2020). Zonal displacement of the Western North Pacific subtropical high from early to late summer. *International Journal of Climatology*, *40*(11), 5029-5041. https://doi.org/10.1002/joc.6508.

Dong, X., Lin, R., & Fan, F. (2017). Comparison of the two modes of the Western Pacific subtropical high between early and late summer. *Atmospheric Science Letters*, *18*(4), 153–160. https://doi.org/10.1002/asl.737.

Feng, J., & Chen, W. (2021). Roles of the north Indian Ocean SST and tropical North Atlantic SST in the latitudinal extension of the anomalous western North Pacific anticyclone during the El Niño decaying summer. *Journal of Climate*, *34*(21), 8503–8517. https://doi.org/10.1175/JCLI-D-20-0802.1.

Feng, J., Chen, W., & Wang, X. (2020). Reintensification of the anomalous western North Pacific anticyclone during the El Niño Modoki decaying summer: Relative importance of tropical Atlantic and Pacific SST anomalies. *Journal of Climate*, *33*(8), 3271–3288. https://doi.org/10.1175/JCLI-D-19-0154.1.

Fosu, B., He, J., & Liguori, G. (2020). Equatorial Pacific warming attenuated by SST warming patterns in the tropical Atlantic and Indian Oceans. *Geophysical Research Letters*, *47*(18), e2020GL088231. https://doi.org/10.1029/2020GL088231.

Guan, W., Hu, H., Ren, X., & Yang, X.-Q. (2019). Subseasonal zonal variability of the western Pacific subtropical high in summer: climate impacts and underlying mechanisms. *Climate Dynamics*, *53*(5), 3325–3344. https://doi.org/10.1007/s00382-019-04705-4.

He, C., & Zhou, T. (2015). Responses of the western North Pacific subtropical high to global warming under RCP4. 5 and RCP8. 5 scenarios projected by 33 CMIP5 models: The dominance of tropical Indian Ocean–tropical western Pacific SST gradient. *Journal of Climate*, *28*(1), 365–380. https://doi.org/10.1175/JCLI-D-13-00494.1.

Hersbach, H., Bell, B., Berrisford, P., Biavati, G., Horányi, A., Muñoz Sabater, J., ... others (2017). Complete ERA5 from 1940: Fifth generation of ECMWF atmospheric reanalyses of the global climate [Dataset]. Copernicus Climate Change Service (C3S) Data Store (CDS). https://doi.org/10.24381/cds.143582cf.

Hersbach, H., Bell, B., Berrisford, P., Hirahara, S., Horányi, A., Muñoz Sabater, J., ... Thépaut, J.-N. (2020). The ERA5 global reanalysis. *Quart. J. Roy. Meteor. Soc.*, *146*(730), 1999-2049. https://doi.org/10.1002/qj.3803.

Hoerling, M. P., Hurrell, J. W., & Xu, T. (2001). Tropical Origins for Recent North Atlantic Climate Change. *Science*, *292*(5514), 90-92. https://www.science.org/doi/abs/10.1126/science.1058582.

Hong, C.-C., Chang, T.-C., & Hsu, H.-H. (2014). Enhanced relationship between the tropical Atlantic SST and the summertime western North Pacific subtropical high after the early 1980s. *Journal of Geophysical Research: Atmospheres*, *119*(7), 3715–3722. https://doi.org/10.1002/2013JD021394.

Hong, C.-C., Lee, M.-Y., Hsu, H.-H., Lin, N.-H., & Tsuang, B.-J. (2015). Tropical SST forcing on the anomalous WNP subtropical high during July–August 2010 and the record-high SST in the tropical Atlantic. *Climate Dynamics*, *45*, 633–650. https://doi.org/10.1007/s00382-014-2275-5.

Hu, S., & Fedorov, A. V. (2020). Indian Ocean warming as a driver of the North Atlantic warming hole. *Nature communications*, *11*(1), 4785. https://doi.org/10.1038/s41467-020-18522-5.

Jiang, L., Chen, H.-C., Li, T., & Chen, L. (2023). Diverse Response of Western North Pacific Anticyclone to Fast-Decay El Niño During Decaying Summer. *Geophysical Research Letters*, *50*(7), e2022GL102612. https://doi.org/10.1029/2022GL102612.

Johnson, Z. F., Chavas, D. R., & Ramsay, H. A. (2022). Statistical framework for western North Pacific tropical cyclone landfall risk through modulation of the western Pacific subtropical high and ENSO. *Journal of Climate*, 1–32. https://doi.org/10.1175/JCLI-D-21-0824.1.

Jones, J. J., Chavas, D. R., & Johnson, Z. F. (2023, November). SST forcing files and Model Builds for ”Inter- basin versus intra-basin sea surface temperature forcing of the Western North Pacific subtropical high’s westward extensions” [Dataset]. Zenodo. https://doi.org/10.5281/zenodo.10127842.

Jong, B.-T., Ting, M., Seager, R., & Anderson, W. B. (2020). ENSO teleconnections and impacts on US summertime temperature during a multiyear La Niña life cycle. *Journal of Climate*, *33*(14), 6009–6024. https://doi.org/10.1175/JCLI-D-19-0701.1.

Kosaka, Y., Xie, S.-P., Lau, N.-C., & Vecchi, G. A. (2013). Origin of seasonal predictability for summer climate over the Northwestern Pacific. *Proceedings of the National Academy of*

Sciences, *110*(19), 7574–7579. https://doi.org/10.1073/pnas.1215582110.

Li, H., Xu, F., & Lin, Y. (2020). The impact of SST on the zonal variability of the western Pacific subtropical high in boreal summer. *Journal of Geophysical Research: Atmospheres*, *125*(11), e2019JD031720. https://doi.org/10.1029/2019JD031720.

Li, T., Wang, B., Wu, B., Zhou, T., Chang, C.-P., & Zhang, R. (2017). Theories on formation of an anomalous anticyclone in western North Pacific during El Niño: A review. *Journal of Meteorological Research*, *31*(6), 987–1006. https://doi.org/10.1007/s13351-017-7147-6.

Li, W., Li, L., Ting, M., & Liu, Y. (2012). Intensification of Northern Hemisphere subtropical highs in a warming climate. *Nature Geoscience*, *5*(11), 830–834. https://doi.org/10.1038/ngeo1590.

Liu, Y., Wu, G., & Ren, R. (2004). Relationship between the subtropical anticyclone and diabatic heating. *Journal of Climate*, *17*(4), 682–698. https://doi.org/10.1175/1520-0442(2004)017%3C0682:RBTSAA%3E2.0.CO;2.

Lu, R. (2001). Interannual variability of the summertime North Pacific subtropical high and its relation to atmospheric convection over the warm pool. *Journal of the Meteorological Society of Japan. Ser. II*, *79*(3), 771–783. https://doi.org/10.2151/jmsj.79.771.

Lu, R., & Dong, B. (2001). Westward extension of North Pacific subtropical high in summer. *Journal of the Meteorological Society of Japan. Ser. II*, *79*(6), 1229–1241. https://doi.org/10.2151/jmsj.79.1229.

Lu, R., & Dong, B. (2005). Impact of Atlantic sea surface temperature anomalies on the summer climate in the western North Pacific during 1997–1998. *Journal of Geophysical Research: Atmospheres*, *110*(D16). https://doi.org/10.1029/2004JD005676.

McGregor, S., Timmermann, A., Stuecker, M. F., England, M. H., Merrifield, M., Jin, F.-F., & Chikamoto, Y. (2014). Recent Walker circulation strengthening and Pacific cooling amplified by Atlantic warming. *Nature Climate Change*, *4*(10), 888–892. https://doi.org/10.1038/nclimate2330.

Park, J.-H., Yeh, S.-W., Kug, J.-S., Yang, Y.-M., Jo, H.-S., Kim, H.-J., & An, S.-I. (2023). Two regimes of inter-basin interactions between the Atlantic and Pacific Oceans on interannual timescales. *npj Climate and Atmospheric Science*, *6*(1), 13. https://doi.org/10.1038/s41612-023-00332-3.

Qian, W., & Shi, J. (2017). Tripole precipitation pattern and SST variations linked with extreme zonal activities of the western Pacific subtropical high. *International Journal of Climatology*, *37*(6), 3018-3035. https://doi.org/10.1002/joc.4897.

Rodwell, M. J., & Hoskins, B. J. (2001). Subtropical anticyclones and summer monsoons. *Journal of Climate*, *14*(15), 3192–3211. https://doi.org/10.1175/1520-0442(2001)014%3C3192:SAASM%3E2.0.CO;2.

Seager, R., Cane, M., Henderson, N., Lee, D.-E., Abernathey, R., & Zhang, H. (2019). Strengthening tropical Pacific zonal sea surface temperature gradient consistent with rising greenhouse gases.

Nature Climate Change, *9*(7), 517–522. https://doi.org/10.1038/s41558-019-0505-x.

Seager, R., Murtugudde, R., Naik, N., Clement, A., Gordon, N., & Miller, J. (2003). Air-Sea Interaction and the Seasonal Cycle of the Subtropical Anticyclones. *Journal of Climate*, *16*(12), 1948 - 1966. https:/doi.org/10.1175/1520-0442(2003)016¡1948:AIATSC¿2.0.CO;2.

UCAR. (2018). Community Earth System Model (Version 2.0) [Software]. University Corporation for Atmospheric Research. https://www.cesm.ucar.edu/models/cesm2/.

Wang, B., Xiang, B., & Lee, J.-Y. (2013). Subtropical high predictability establishes a promising way for monsoon and tropical storm predictions. *Proceedings of the National Academy of Sciences*, *110*(8), 2718–2722. https://doi.org/10.1073/pnas.1214626110.

Wang, X., Li, T., & He, C. (2021). Impact of the Mean State on El Niño–Induced Western North Pacific Anomalous Anticyclones during El Niño Decaying Summer in AMIP Models. *Journal of Climate*, *34*(22), 9201–9217. https://doi.org/10.1175/JCLI-D-20-0747.1.

Williams, I. N., & Patricola, C. M. (2018). Diversity of ENSO Events Unified by Convective Threshold Sea Surface Temperature: A Nonlinear ENSO Index. *Geophysical Research Letters*, *45*(17), 9236-9244. https://doi.org/10.1029/2018GL079203.

Wu, B., Li, T., & Zhou, T. (2010). Relative Contributions of the Indian Ocean and Local SST Anomalies to the Maintenance of the Western North Pacific Anomalous Anticyclone during the El Niño Decaying Summer. *Journal of Climate*, *23*(11), 2974 - 2986. https://doi.org/10.1175/2010JCLI3300.1.

Wu, Q., Wang, X., & Tao, L. (2020). Interannual and interdecadal impact of Western North Pacific Subtropical High on tropical cyclone activity. *Climate Dynamics*, *54*(3), 2237–2248. https://doi.org/10.1007/s00382-019-05110-7.

Xie, S.-P., Hu, K., Hafner, J., Tokinaga, H., Du, Y., Huang, G., & Sampe, T. (2009). Indian Ocean capacitor effect on Indo–western Pacific climate during the summer following El Niño. *Journal of climate*, *22*(3), 730–747. https://doi.org/10.1175/2008JCLI2544.1.

Xie, S.-P., Kosaka, Y., Du, Y., Hu, K., Chowdary, J. S., & Huang, G. (2016). Indo-western Pacific Ocean capacitor and coherent climate anomalies in post-ENSO summer: A review. *Advances in Atmospheric Sciences*, *33*(4), 411–432. https://doi.org/10.1007/s00376-015-5192-6.

Yuan, Y., & Yan, H. (2013). Different types of La Niña events and different responses of the tropical atmosphere. *Chinese Science Bulletin*, *58*, 406–415. https://doi.org/10.1007/s11434-012-5423-5.

Zhou, T., Yu, R., Zhang, J., Drange, H., Cassou, C., Deser, C., … others (2009). Why the western Pacific subtropical high has extended westward since the late 1970s. *Journal of Climate*, *22*(8), 2199–2215. https://doi.org/10.1175/2008JCLI2527.1.

Zuo, J., Li, W., Sun, C., & Ren, H.-C. (2019). Remote forcing of the northern tropical Atlantic SST anomalies on the western North Pacific anomalous anticyclone. *Climate Dynamics*, *52*, 2837–2853. https://doi.org/10.1007/s00382-018-4298-9.

Figure 1.

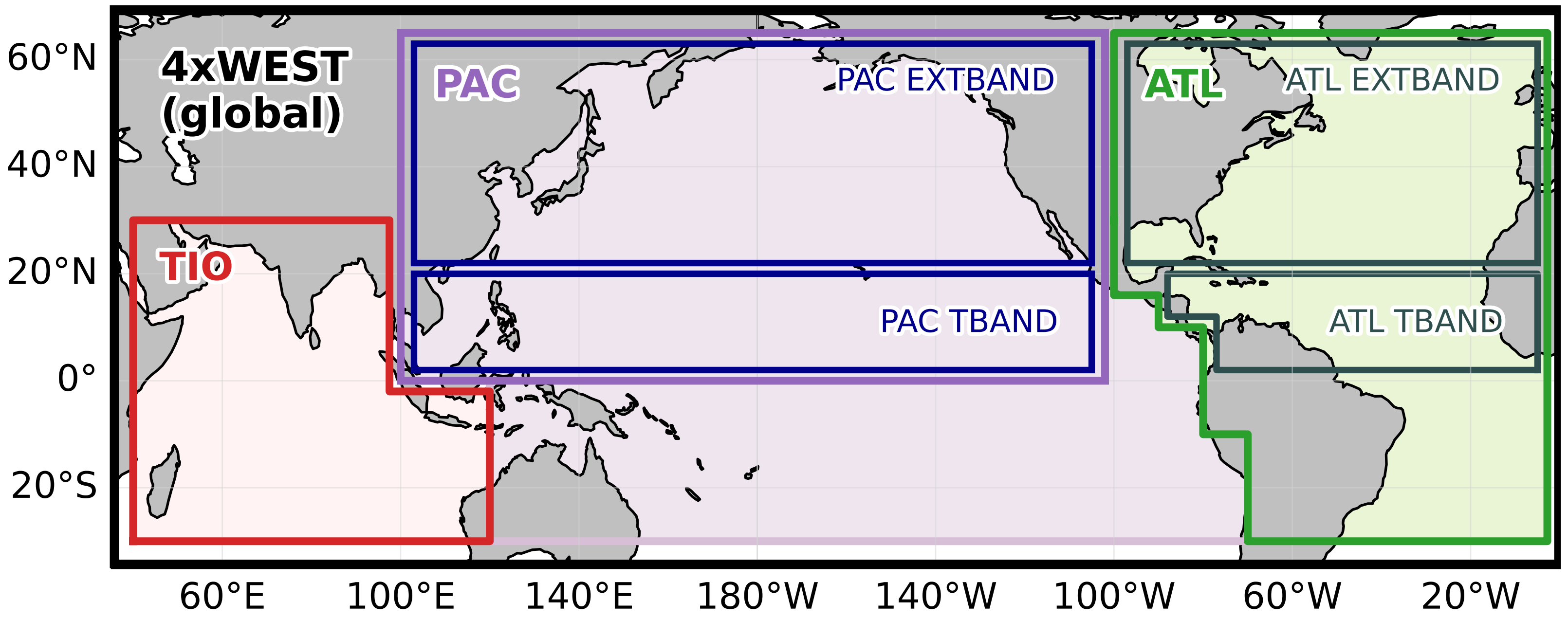
4xWEST
(global)
PAC
PAC EXTBAND
PAC TBAND
ATL
ATL EXTBAND
ATL TBAND
TIO
60°N
40°N
20°N
0°
20°S
60°E
100°E
140°E
180°W
140°W
100°W
60°W
20°W

Figure 2.

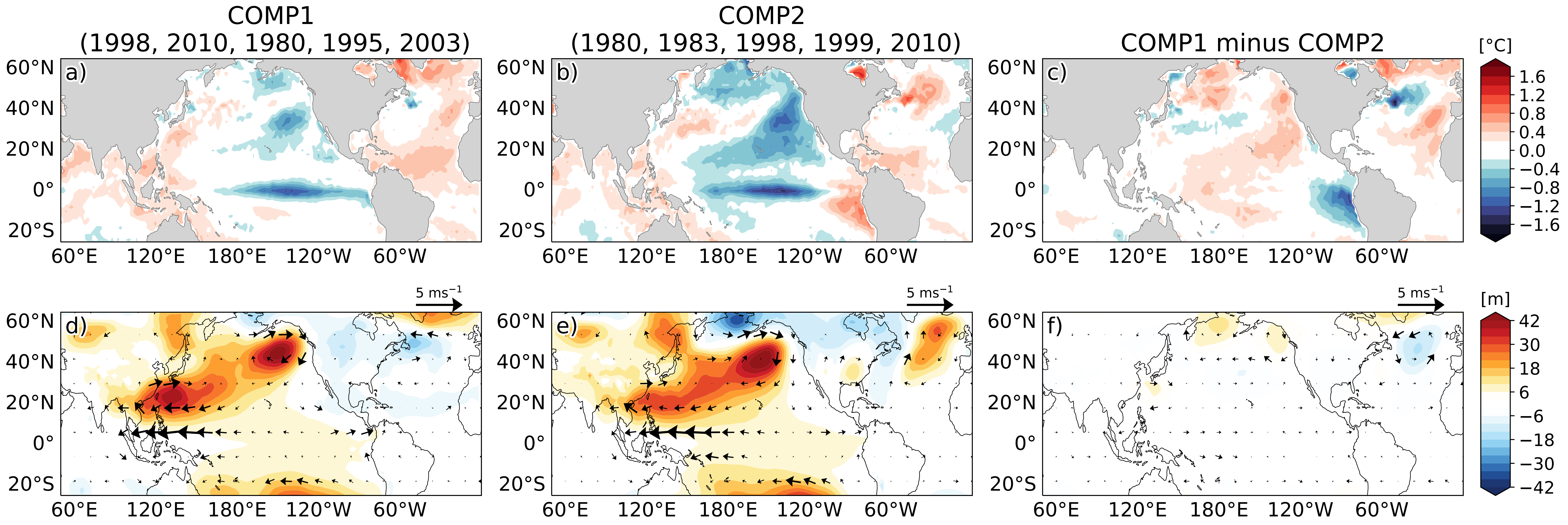
COMP1
(1998, 2010, 1980, 1995, 2003)
COMP2
(1980, 1983, 1998, 1999, 2010)
COMP1 minus COMP2
[°C]
1.6
1.2
0.8
0.4
0.0
−0.4
−0.8
−1.2
−1.6
a)
b)
c)
d)
e)
f)
60°N
40°N
20°N
0°
20°S
60°E
120°E
180°E
120°W
60°W
5 ms−1
[m]
42
30
18
6
−6
−18
−30
−42

Figure 3.

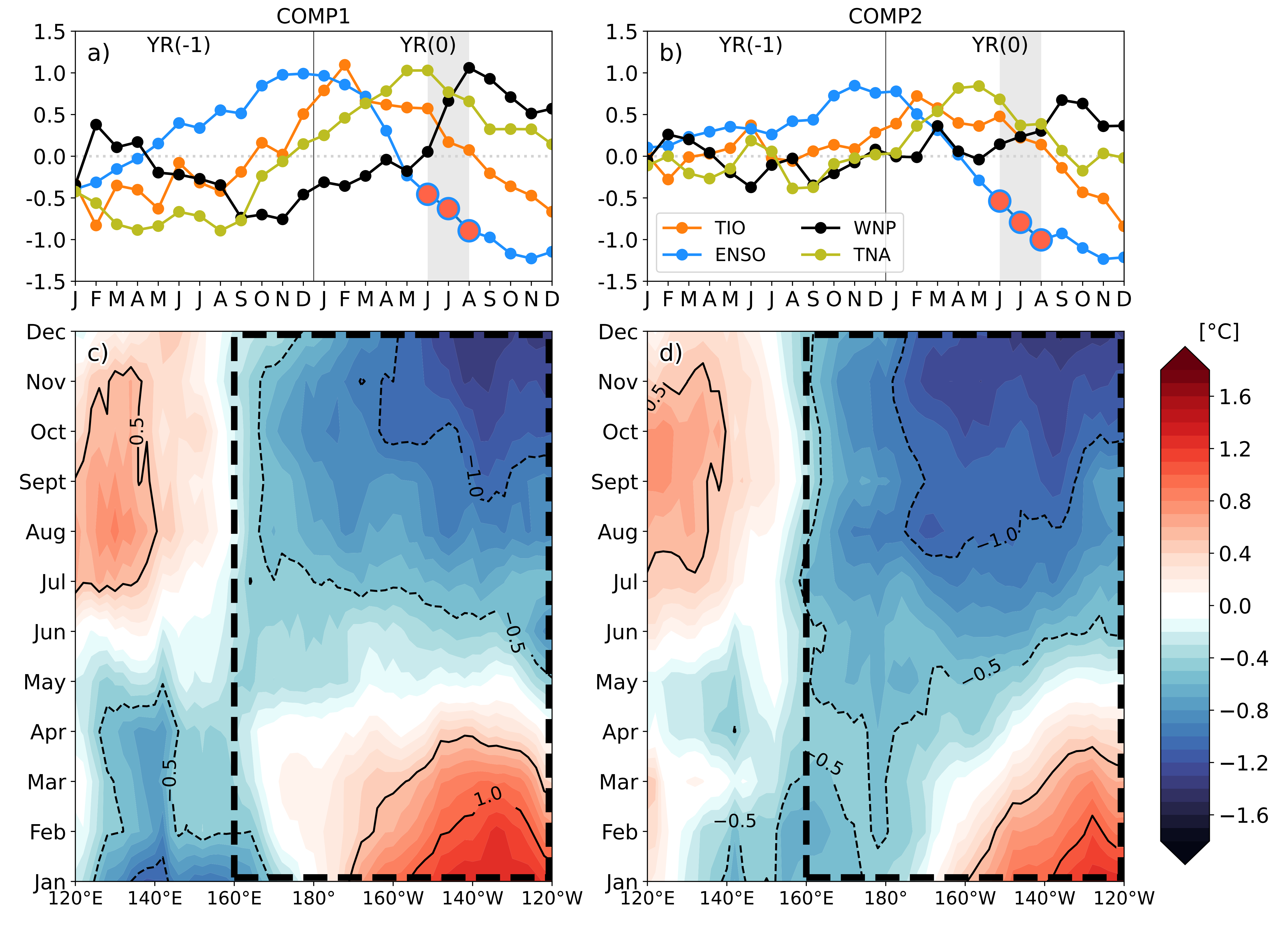

COMP1
COMP2
a)
b)
c)
d)
YR(-1)
YR(0)
TIO
ENSO
WNP
TNA
J F M A M J J A S O N D J F M A M J J A S O N D
Dec
Nov
Oct
Sept
Aug
Jul
Jun
May
Apr
Mar
Feb
Jan
120°E 140°E 160°E 180° 160°W 140°W 120°W
[°C]
1.6
1.2
0.8
0.4
0.0
−0.4
−0.8
−1.2
−1.6

Figure 4.

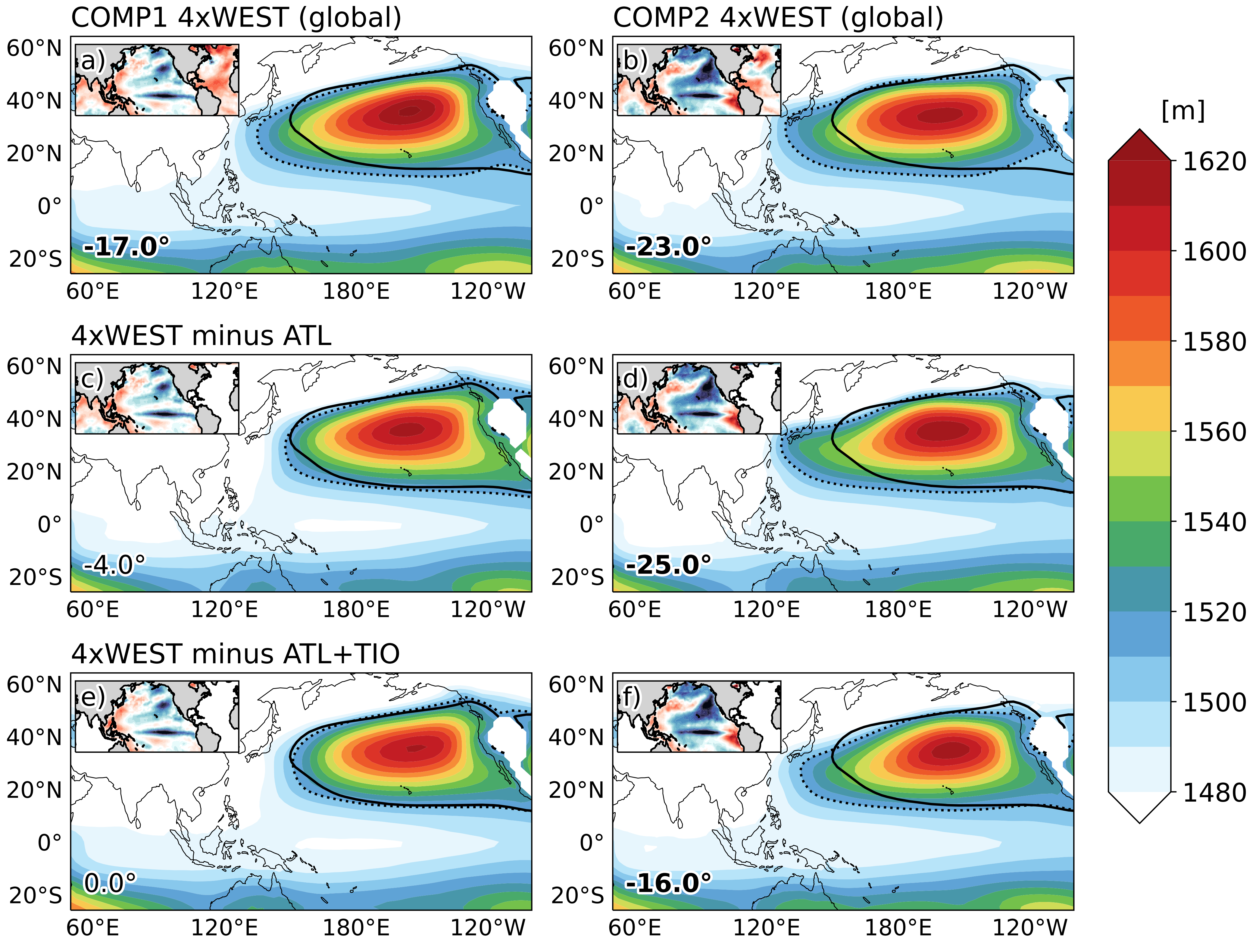
COMP1 4xWEST (global)
COMP2 4xWEST (global)
4xWEST minus ATL
4xWEST minus ATL+TIO
a)
b)
c)
d)
e)
f)
-17.0°
-23.0°
-4.0°
-25.0°
0.0°
-16.0°
60°N
40°N
20°N
0°
20°S
60°E
120°E
180°E
120°W
[m]
1620
1600
1580
1560
1540
1520
1500
1480

Figure 5.

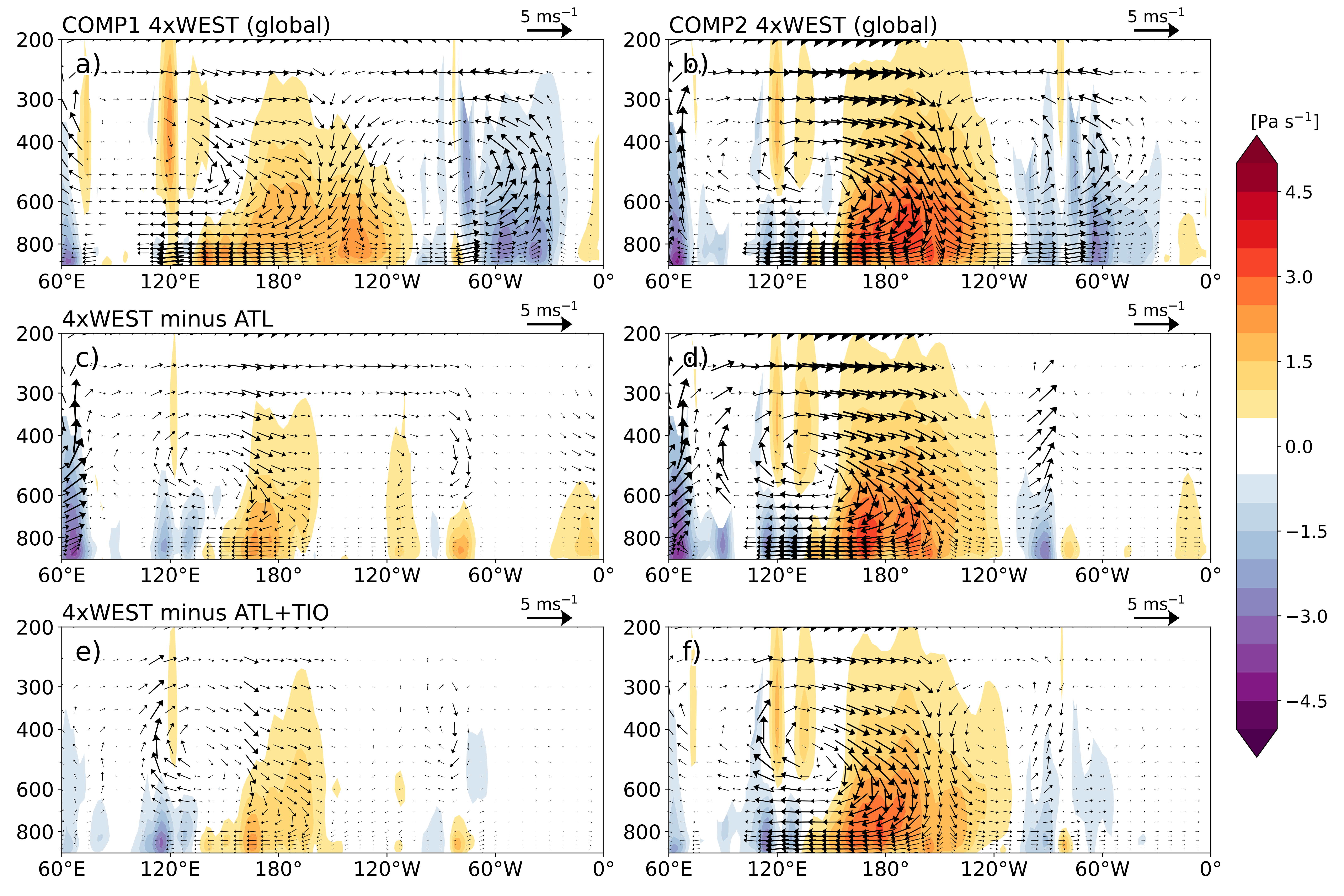

COMP1 4xWEST (global)
COMP2 4xWEST (global)
4xWEST minus ATL
4xWEST minus ATL+TIO
a)
b)
c)
d)
e)
f)
5 ms−1
200
300
400
600
800
60°E
120°E
180°
120°W
60°W
0°
[Pa s−1]
4.5
3.0
1.5
0.0
−1.5
−3.0
−4.5

Figure 6.

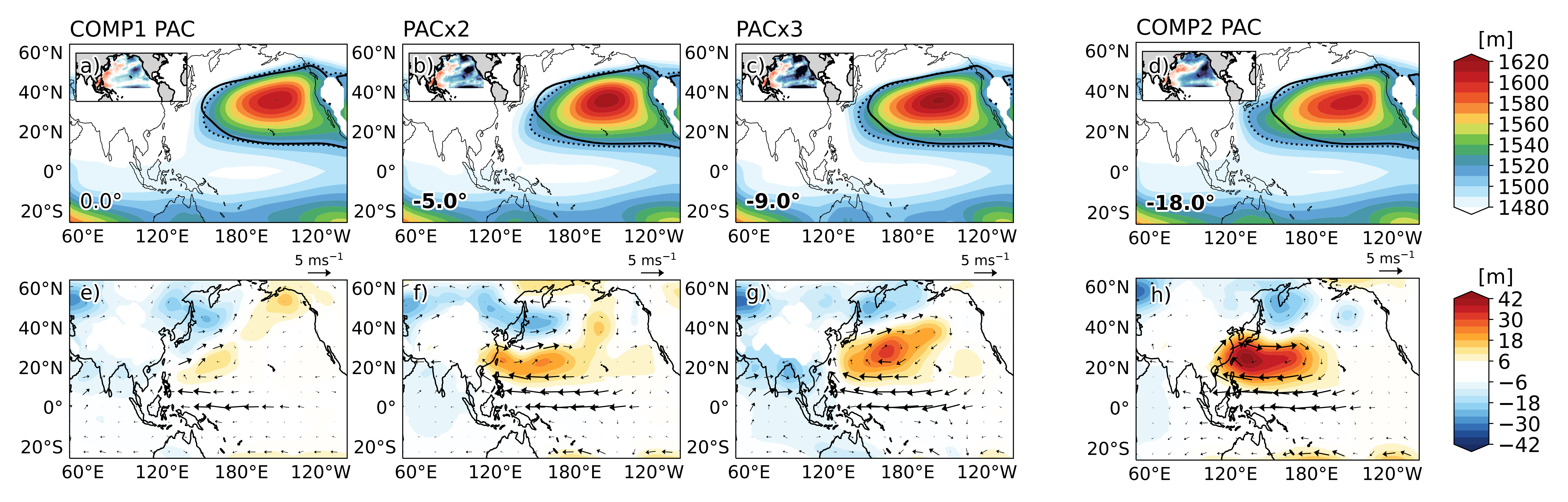

COMP1 PAC
PACx2
PACx3
COMP2 PAC
a)
b)
c)
d)
e)
f)
g)
h)
0.0°
-5.0°
-9.0°
-18.0°
60°N
40°N
20°N
0°
20°S
60°E
120°E
180°E
120°W
5 ms^{-1}
[m]
1620
1600
1580
1560
1540
1520
1500
1480
[m]
42
30
18
6
−6
−18
−30
−42

Figure 7.

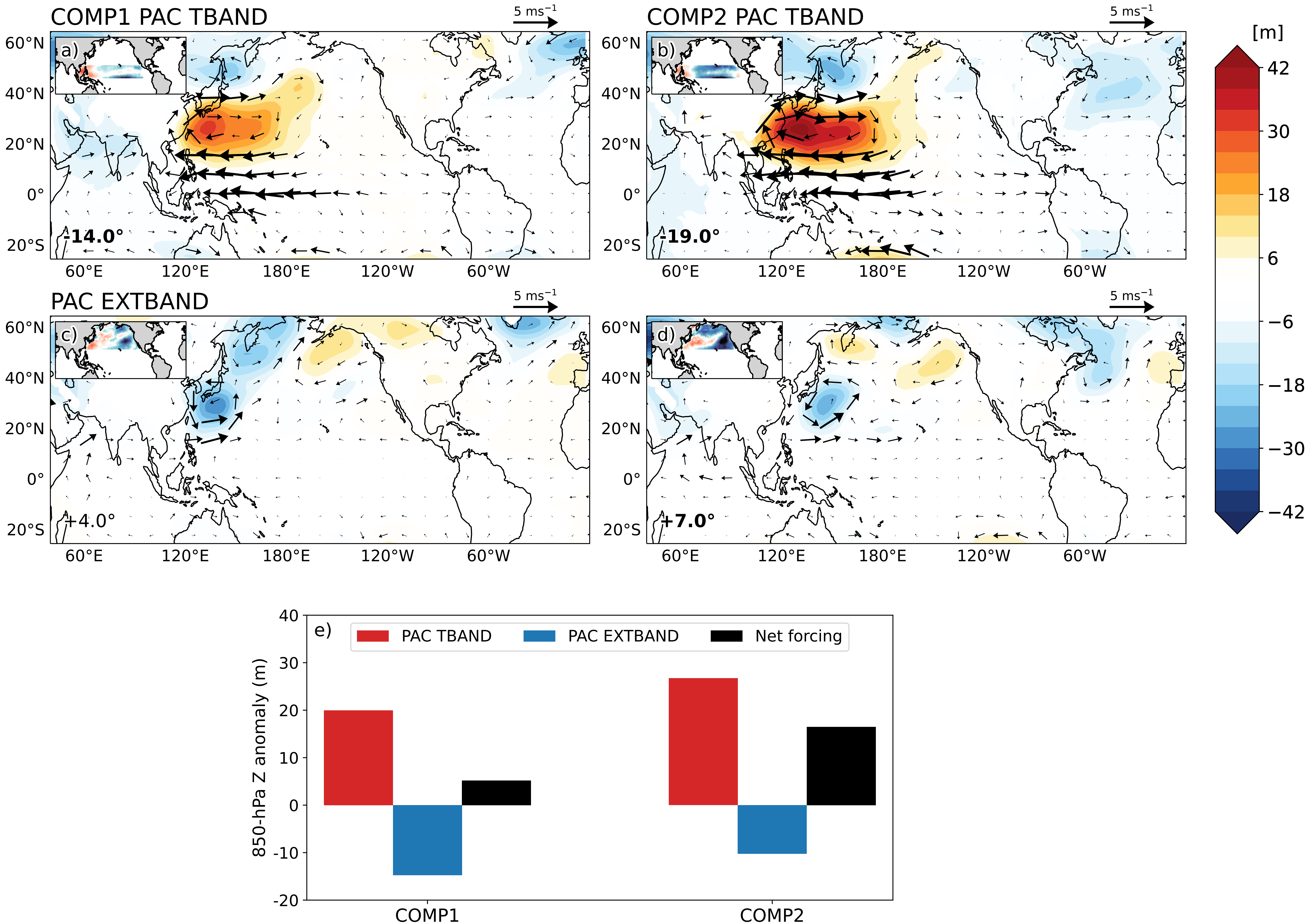

COMP1 PAC TBAND
COMP2 PAC TBAND
PAC EXTBAND
a)
b)
c)
d)
5 ms^{-1}
-14.0°
-19.0°
+4.0°
+7.0°
60°N
40°N
20°N
0°
20°S
60°E
120°E
180°E
120°W
60°W
[m]
42
30
18
6
−6
−18
−30
−42
e)
PAC TBAND
PAC EXTBAND
Net forcing
850-hPa Z anomaly (m)
40
30
20
10
0
-10
-20
COMP1
COMP2

Figure 8.

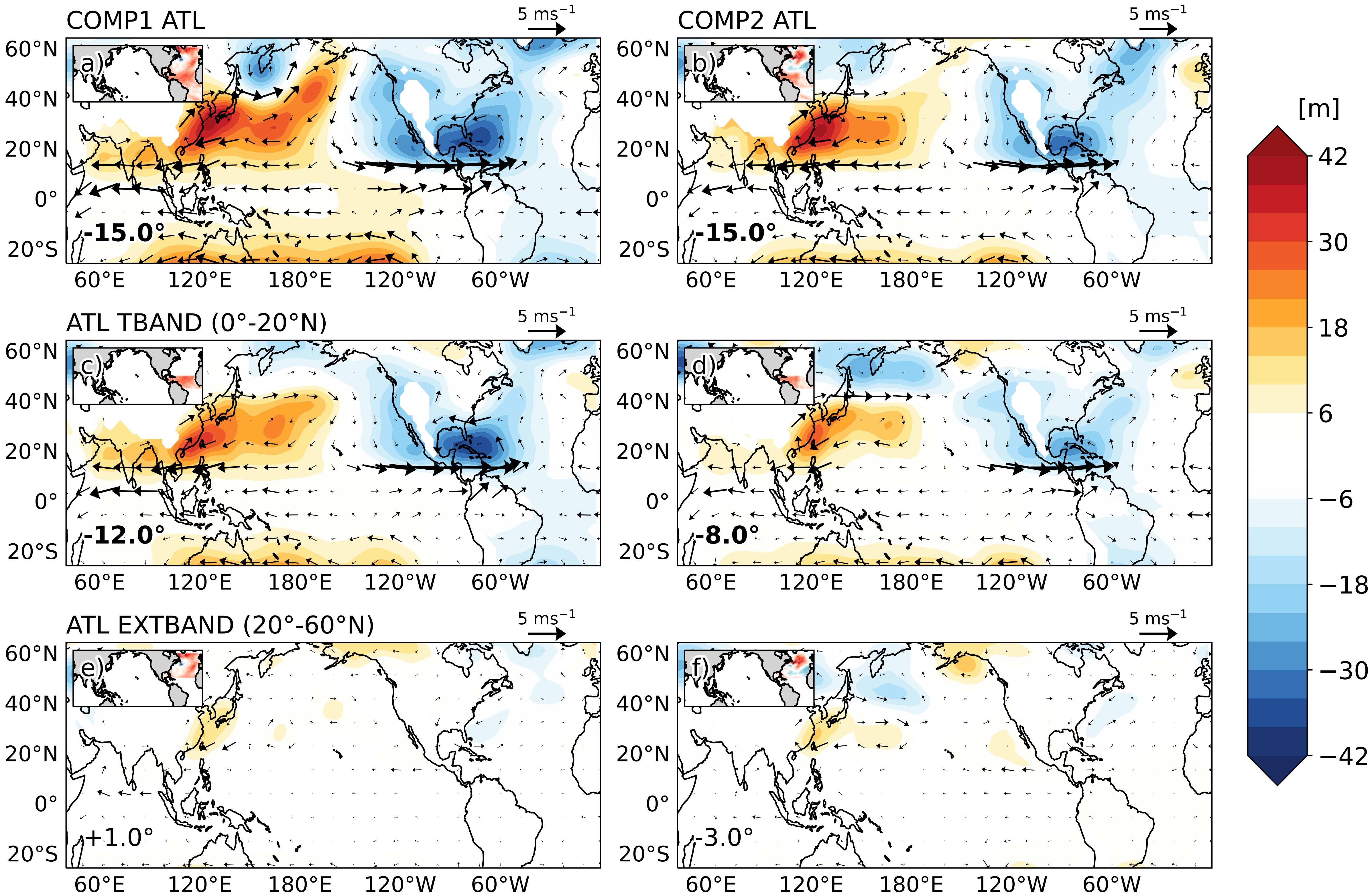
COMP1 ATL
COMP2 ATL
ATL TBAND (0°-20°N)
ATL EXTBAND (20°-60°N)
5 ms^{-1}
a)
b)
c)
d)
e)
f)
-15.0°
-15.0°
-12.0°
-8.0°
+1.0°
-3.0°
60°N
40°N
20°N
0°
20°S
60°E
120°E
180°E
120°W
60°W
[m]
42
30
18
6
−6
−18
−30
−42